Alma Mater Studiorum – Università di Bologna

DOTTORATO DI RICERCA IN

MECCANICA E SCIENZE AVANZATE DELL'INGEGNERIA

CICLO XXVIII

Settore Concorsuale di afferenza:
09/A2 - MECCANICA APPLICATA ALLE MACCHINE

Settore Scientifico disciplinare:
ING-IND/13 - MECCANICA APPLICATA ALLE MACCHINE

New Solutions for the Modelling and Design of a Hand Exoskeleton System

Presentata da:
CLAUDIO MAZZOTTI

Coordinatore Dottorato:
PROF. VINCENZO PARENTI CASTELLI

Relatore:
PROF. VINCENZO PARENTI CASTELLI

Esame finale anno 2016

To Irene

Keywords

- *Hand exoskeleton;*
- *Robotic rehabilitation;*
- *Synthesis of mechanisms;*
- *Joint axis identification.*

Acknowledgements

First of all, I would like to thank Prof. Vincenzo Parenti Castelli, for the opportunity he gave me to consolidate my studies, for his support during these years and for the useful discussions that made me grow professionally and personally.

I thank Dr. Marco Troncossi for his support and the precious assistance he gave me, especially during the first years of this work experience. I would also like to thank very much Dr. Nicola Sancisi, in particular for the last year working together, during which I could develop a real passion for Research.

Finally, special thanks to my friends Alessandro, Margherita, Fabrizio, Francesco, Irene, Luca, Federica, Michele, Antonio and Troy!

Summary

List of Figures

List of Tables

Abstract

In the last decades, a worldwide interest in research was focused on human-machine interaction. In particular, a growing attention was placed on robotic rehabilitation devices. Recently, a prototype of a hand exoskeleton for post-stroke rehabilitation purpose was proposed by the Group of Robotics, Automation and Articular Biomechanics (GRAB) at the Department of Industrial Engineering, University of Bologna. The prototype comprises five planar 1 Degree-of-Freedom (DoF) mechanisms (one per finger) globally actuated by two DC motors. The first motor simultaneously actuate the flexion/extension motion of the index, the middle, the ring and the little finger, whereas the second motor only actuates the flexion/extension motion of the thumb. Each finger mechanism is directly connected with the human finger by Velcro® strips at the level of each finger phalange (except for the first phalange of the thumb), in addition a further strip connects the device to the human palm, thus a total of fifteen human-machine connections are needed to fasten the device to the patient hand. The moving link of the thumb mechanism is actuated by a spatial RSSR mechanism whose frame link geometry must be ad hoc regulated every time the device is fitted on a new patient hand. In other words, the frame link geometry of the RSSR mechanism changes according to the patient hand size.

In this dissertation, some problems arose from the study of the hand exoskeleton prototype proposed by the GRAB are tackled with the aim to solve them in order to design a new version of the device.

The first problem regards the high number of human-machine connections needed to fasten the device to the patient hand. This problem was overcome by proposing a new planar 1-DoF finger mechanism based on a Stephenson type

chain that permits to lower the total number of human-machine connections from fifteen to only six. The synthesis of this finger mechanism is reported and several simulations, with the aim to evaluate the behavior of the finger mechanism once fitted on hands having different sizes, are conducted.
The second problem regards the need to synthesize the RSSR mechanism in order to guarantee the optimal motion and force transmission to the thumb mechanism once the hand exoskeleton is fitted to a new patient, i.e. for different frame link geometries of the RSSR mechanism. From this second problem, a novel synthesis procedure for the optimal motion and force transmission of a RSSR mechanism characterized by having a fixed link length of the floating links and variable frame link geometry is presented. The synthesis procedure is firstly presented in a general way, and then applied to the particular case of the hand exoskeleton device here studied. Results show that an optimal RSSR mechanism can be found for a small range of frame link geometries and thus several considerations for a compromise solution are discussed.
The third problem regards the need to have a reliable model of the human hand in order to best design the overall device. The first step toward a model of the human hand is to model each finger as a serial manipulator and to assume that the flexion/extension motion of two adjacent bones of the finger can be modelled as a rotation about a revolute axis. Given this interest, two novel axes identification techniques are here presented. These techniques are based on the Burmester theory (i.e., a theory generally used for the synthesis of mechanisms), which is here used in an original way to identify an axis of rotation. Experimental tests, devoted to measure in vivo the spatial motion of the human fingers, are conducted and the relative motion between adjacent bones of the human finger is obtained. Finally, the axes identification techniques are applied and the results are discussed.

This dissertation reports different solutions for the modelling and design of a new version of the hand exoskeleton proposed by the GRAB, but it is worth noting that the problems here tackled and the solutions found are of general interest, thus going beyond the scope of this thesis.

Chapter 1

Introduction and objectives of the thesis

1.1 Post-stroke rehabilitation: hand exoskeletons

In Italy stroke affects about 200,000 people per year and it is the leading cause of disability and the third leading cause of mortality (Consoli et al., 2010). The 35% of the persons affected by stroke suffers from brain-damage-related disabilities e.g. lack of control of the arm and/or the hand. Traditional rehabilitation with a therapist is nowadays the more common way to rehabilitate stroke patients. The results obtained from the rehabilitation therapy are better and better if the rehabilitation training is more intensive and continuous in time (Heo et al., 2012). However traditional rehabilitation requires manual interaction of the therapist with the patient, consequently raising times and costs. These drawbacks, in addition to the lack of quantitative evaluations of patient improvements during the rehabilitation process, make the traditional rehabilitation approach not completely satisfying and successful. In the last decades, robotic rehabilitation gained a great interest as a useful tool to assist therapists during the rehabilitation of stroke patients (Chang and Kim, 2013). The possibility to provide repetitive trainings, to assist-as-needed the patients (Marchal-Crespo and Reinkensmeyer, 2009) during exercises and to quantitatively evaluate the improvements reached by the patients during the rehabilitation therapy represents the main advantages of the robotic

rehabilitation. Nowadays, exoskeletons can be efficiently used as rehabilitation systems. In this dissertation the focus is on hand exoskeleton rehabilitation systems, also known as active ortheses. Recently, many prototypes of hand exoskeletons have been proposed in the literature (Mozaffari et al., 2011; Heo et al., 2012). From the literature it is clear that the solutions proposed to guide the motion of each finger are the most varied. Many solutions exploit the use of mechanisms coupled to the human fingers to guide the motion of the fingers themselves. Usually, the adopted mechanisms have more than 1 degree-of-freedom (DoF) then they use more than one actuator to guide the motion of each finger, resulting in complex and bulky multi-DoF hand exoskeletons which consequently increase the final cost of the devices. Several authors have pursued different design strategies proposing hand exoskeletons with simple architectures and a lower number of actuators. In particular, we highlight the hand device of the Gentle-G (Loureiro and Harwin, 2007) that uses one actuator for the thumb and two actuators for the four finger together, the robot proposed by Masia et al. (2007) that allows finger and thumb extension to be controlled by the same single DoF, the HWARD (Takahashi et al., 2008) that has one actuator for the four fingers together, the active hand orthosis proposed by Rosati et al. (2009) that uses a 1-DoF four bar linkage mechanism that actuate the four fingers together. In addition, Wolbrecht et al. (2011) proposed an eight-link 1-DoF mechanism designed for finger rehabilitation, and Yihun et al. (2012) proposed a six-link spatial 1-DoF mechanism designed for the thumb motion guidance. Finally, two recent papers (Troncossi et al., 2012; Mozaffari et al., 2013) proposed a hand exoskeleton that comprises a 1-DoF planar mechanism for each finger using one actuator for the thumb motion guidance and another actuator for the simultaneous motion guidance of the four fingers together. In the following Section a deep focus on this last hand exoskeleton is reported.

1.2 The Bologna Hand Orthoses (BHO)

Recently, a prototype of a hand exoskeleton (Troncossi et al, 2012; Mozaffari and Troncossi, 2013; and Mozaffari, 2013) called Bologna Hand Orthoses (BHO hereinafter) was proposed by the Group of Robotics, Automation and Articular Biomechanics (GRAB) at the Department of Industrial Engineering,

University of Bologna. In this section a description of this device was reported with the aim to: (i) give a briefly description of the design specifications who guided the whole project, and (ii) to highlight some practical considerations on the final prototype useful for a future version of such a prototype itself. From these considerations arose three different problems, reported in Chapters 2, 3 and 4 respectively, whose solution represent the core of the work reported in this dissertation.

1.2.1 Design specifications of the BHO project

Precise design specifications guided the overall project of the BHO, and are here briefly summarized. First of all, the intended application of the hand exoskeleton is to rehabilitate the human hand motion capability of post-stroke patients. In particular, the device is intended to be used for an assist-as-needed rehabilitation protocol thanks to witch both the following patient ability: the flexion/extension of each finger and the power grasping of cylindrical objects, have to be rehabilitated. The main high-level design choice is to design a two degree-of-actuation device, i.e. a device equipped with two independent actuators. In particular one actuator is intended to actuate the flexion/extension simultaneous motion of the four fingers together, whereas the second actuator is intended for the flexion/extension motion of the thumb. The movement of each human finger is driven by a one Degree-of-Freedom (DoF) planar mechanism (called finger mechanism hereinafter) fixed to the finger itself, whereas the opposition/anteposition of the thumb is adjusted manually. The abduction/adduction of each finger is disregarded. Each finger mechanism, and in general the whole device, is fixed above the hand in such a way as to guarantee the interaction of the human hand with the cylindrical objects have to be grasped. Since the device is devoted to rehabilitation purpose, the safe of the patient is mandatory, thus mechanical brakes to limit the flexion/extension of each finger must be considered. Finally, high-resolution encoders must be embedded in the device in order to implement a closed-loop control in operation of the hand exoskeleton.

1.2.2 Description of the BHO prototype

In this section the built prototype of the BHO is here briefly presented.
Figure 1.1 shows a CAD view of the BHO, whereas Figure 1.2 shows two

pictures of the built prototype. The device is mainly composed by five planar mechanisms, one per finger globally actuated by two electrical DC motors.

The mechanisms that guide the motion of the four fingers (index, middle, ring and little), labelled as FMs in Figure 1.1, are based on the same kinematic architecture: they comprise 12 links interconnected by 16 revolute joints. As regards the thumb, it was decided to keep the first phalange as fix, thus the thumb mechanism (labelled as TM) comprises just 8 links and 11 revolute joints. For both the 12-link and the 8-link mechanisms, the human phalanges and the anatomical articulations are part of the mechanism.

Each mechanism is placed above the human finger and it is connected to the finger itself by Velcro® strings at the level of each human phalange. As regard the actuation, the first motor (labelled as M_1), drives the four FMs simultaneously. The moving link of each FM is fixed to the shaft S, and the power flow comes from the motor M_1 to the shaft S (and thus to the FMs) through the gear G_1. The second actuator (labelled as M_2), drives the TM. The motion transmission from M_2 to the moving link of the TM is achieved by using a 1-DoF spatial four bar linkage, also known as RSSR mechanism, where R and

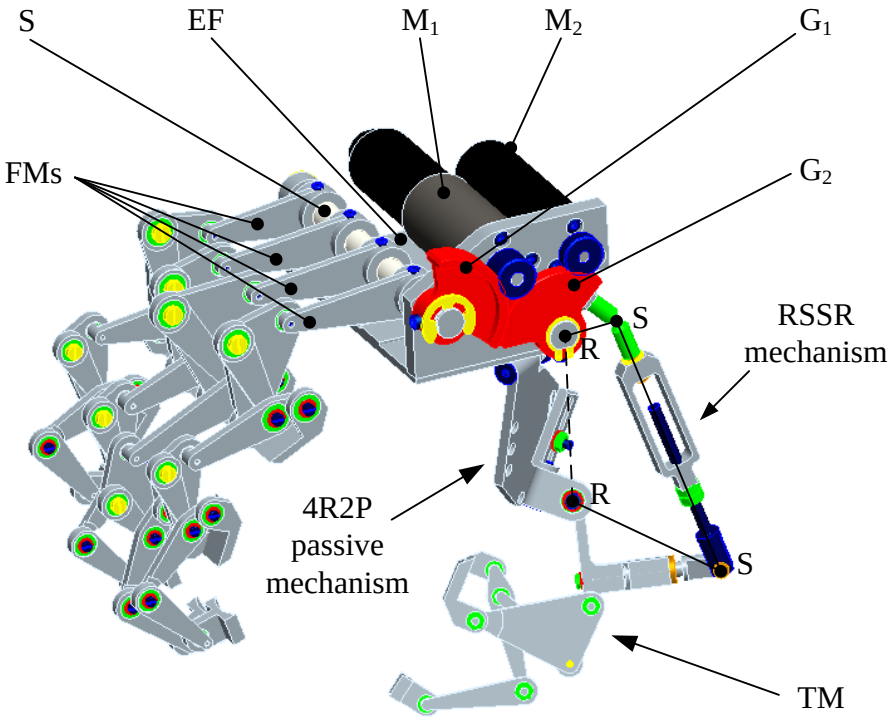

Figure 1.1 CAD view of the BHO.

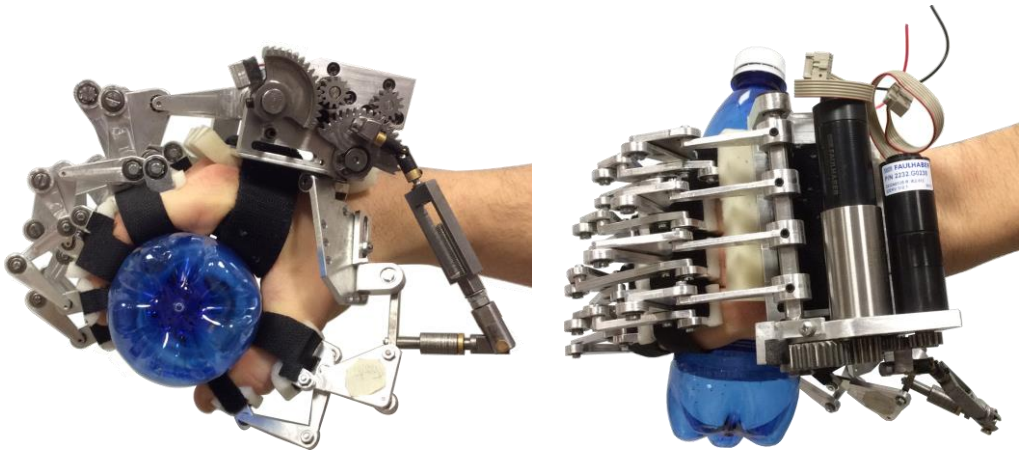

Figure 1.2 The BHO built prototype.

S stand for revolute and spherical kinematic pair respectively. The moving link of the RSSR mechanism is driven by the gear G_2 (which is connected to the actuator M_2), whereas the follower link of the RSSR is connected to the moving link of the TM. The two DC motors, mounted on a rigid frame (labelled as EF) placed on the back side of the hand, are fastened to the hand by a single Velcro® string. Thus, a total of 15 Velcro® connections (i.e. 12 connections for the FMs, 2 connections for the TM and 1 connection for the EF) are needed to fasten the exoskeleton to the patient hand.

As stated in the design specification, it was decided to keep the first phalange of the human thumb fixed in a given pose. As a consequence, the motion plane of the thumb mechanism doesn't change during the flexion/extension motion-in-operation of the thumb. In general, the motion plane of the thumb mechanism must be properly regulated according to the patient hand anthropometric geometry. In order to choose the better motion plane, a 4R2P (where R and P stand for revolute and prismatic joint respectively) 6-DoFs mechanism with passive joints was used. The 6-DoFs passive mechanism is fixed to both the frame (EF) of the exoskeleton and to the first phalange of the thumb. The configuration of the 4R2P mechanism can be manually adjusted and fixed during the fitting procedure of the hand exoskeleton to the patient hand. The frame link of the RSSR mechanism coincides with the 4R2P mechanism. As a result, if the geometry of the 4R2P passive mechanism have to be adjusted during the fitting procedure, the frame link of the RSSR mechanism consequently change, and in general the kinematic

motion transmission characteristics of the RSSR mechanism move away from the optimal operating conditions. The link length of the coupler link of the RSSR mechanism, i.e. the connecting rod between the two spherical joints, can be manually regulated in order to provide the optimal motion and force transmissibility for different patients.

1.2.3 Design challenges arising from the BHO prototype

Several test conducted on the built prototype (Mozaffari, 2013; Loconsole et al., 2013; Leonardis et al., 2015) show that the BHO fully satisfies all the requirements imposed by the design specifications. The final prototype was low weight, powerful and satisfactorily guides the motion of each finger for the power grasping tasks. In the following, several considerations arising from the study of the final prototype are reported with the aim to highlight some challenging problems to be solved for a future version of the BHO device.

The first consideration regards the high number of human-machine connections. From the practical point of view, to fasten 15 Velcro® strings to the patient hand is quite complicated and a time consuming procedure. In this perspective, a possible improvement of the BHO may be to reduce the number of human-machine connections. Maintaining the same strategies adopted for the BHO, i.e. to guide each finger by a planar mechanism, the challenge is to find a new mechanism that need of a fewer number of human-machine connections per finger. This problem is treated in the Chapter 2.

The second consideration arises from the need to adjust both the 4R2P geometry and the coupler link length. Once again, from the practical point of view, this double-regulation procedure is time consuming and it is difficult to find the best coupler link length as well. As a result, a non-optimal motion and force transmission of the RSSR mechanism to the thumb mechanism may occur. In this perspective, a possible improvement may be to reduce the number of regulation needed in the fitting procedure. In particular, the best choice may be to maintain the passive regulation of the 4R2P mechanism disregarding the RSSR coupler link length regulation. The problem thus reduces to synthesize an RSSR mechanism characterized by the fact that the motion and force transmission quality must be optimal for all the possible frame link geometries arising from the 4R2P regulation. This problem is treated in the Chapter 3.

The final consideration arises from the need to have a reliable mathematical

model of the hand motion in order to predict the configuration assumed by each finger around the cylinder to grasp. Generally speaking, a model is useful for the optimal synthesis of each finger mechanism and for the study of the synchronized motion of the fingers around the cylinder to grasp. As a first step toward a model of the human hand was to model each finger as a serial manipulator and to assume that the flexion/extension motion of two adjacent bones of each finger can be modelled as a rotation about a revolute axis. In this perspective, two novel joint axes identification techniques based on the Burmester theory were presented. The Burmester theory is generally used for the synthesis of mechanisms, but it is here used in an original way to identify an axis of rotation. This problem is treated in the Chapter 4.

Chapter 2

Design of a new finger exoskeleton for a lower number of human-machine connections

2.1 Introduction

As stated in Chapter 1, the final goal of the research activity conducted by the Group of Robotics, Automation and Articular Biomechanics (GRAB), is to design a new hand exoskeleton for rehabilitation purposes, which could possibly represent a good trade-off among simplicity, functionality and cost. In particular, the rehabilitation target is to drive the motion of the human finger in order to execute a classical post stroke rehabilitation task: the power grasping of cylindrical objects. This particular task was chosen as a reference task because rehabilitation of power grasping is, in general, one of the main manipulation ability that stroke patients need to recover first. To achieve this goal, several preliminary choices have to be taken into account by the designer. In (Troncossi et al, 2012a-b) a systematic analysis of the principles ruling the design process of hand exoskeletons is reported. Generally speaking, the design of a hand exoskeleton must face a wide range of choices, such as: the solution used for the motion guidance of each finger, the number of actuators, the motion transmission system, the control scheme, etc. The *best possible device* has probably not been invented yet and a trade-off must be found. In Mozaffari and Troncossi (2013) is shown that a good trade-off could be found by adopting the following strategies: (*i*) the use of a 1-DoF mechanism to guide the motion of

each finger, (*ii*) to place the mechanism above the finger in order to avoid interferences between the hand exoskeleton and the cylinder to grasp (*iii*) the use of two actuators only, one to actuate the thumb motion and the other one to actuate the four finger simultaneously. As a final result the hand exoskeleton device should be a good compromise among simplicity, functionality and costs. The BHO device (recalled in Section 1.2) was built according to this particular design philosophy and the resulting prototype fully satisfies the expectations (Mozaffari, 2013; Leonardis et al., 2015).

In Section 1.2 of this dissertation, some considerations on the final BHO prototype were reported with the aim to highlight some new challenging problems to be tackled for a future version of the BHO. Particularly interesting for the aim of this Chapter is the consideration regarding the high number of human-machine connections needed to fasten the BHO to the patient hand. In order to tackle this problem, a new solution to reduce the number of human-machine connections is here presented. The proposed solution is to adopt a new mechanism for the finger guidance of the five fingers. In particular, this Chapter deals with the design of a 1 DoF Stephenson type mechanism (i.e. a 6-link mechanism) for a finger exoskeleton. The finger exoskeleton, fastened to the second phalange of the human finger and to the palm, guides the flexion/extension motion of the finger while generating desired grasping trajectories. Preliminary results and a 3D printed prototype of the proposed finger exoskeleton are reported. The results obtained showed that the proposed finger exoskeleton can be successfully adopted for the motion guidance of the fingers of a hand exoskeleton; moreover, since for the 6-link mechanism only one human-machine connection per finger is necessary, in case the actual 12-link mechanism used for the BHO will be replaced by the 6-link mechanism here studied, the total number of human-machine connections drops to five, i.e. one per finger.

2.2 Design of the new finger exoskeleton

The design of the finger exoskeleton is reported in this Section; it is divided in three steps, the first step concerns the choice of a hand grasping model, the second step concerns the choice of the mechanism used to guide the motion of the finger, whereas the third step concerns the synthesis of the selected

mechanism.

2.2.1 The grasping model

According to a conventional model, the human hand has 20 DoFs (Kapandji, 1982; Buchholz et al., 1992). Each finger is usually modelled as a 4-DoF serial manipulator. The first DoF exploits the abduction/adduction motion of the first phalanx with respect to the hand metacarpus, whereas the other three DoFs exploit the flexion/extension motion of the three phalanges of each finger. As universally accepted, a simplification of the complex motion of the hand is to consider the three flexion/extension revolute axis as parallel lines (Buchholz and Armstrong 1992; Bullock et al., 2012). In this Chapter a grasping model inspired to the one proposed in Burton et al (2011) is used. In Buchholz et al (1992) the model of the human hand is obtained by considering the phalanges as rigid links and the relative motion of two adjacent phalanges is considered as a rotation about an axis passing through the MCP, the PIP and the DIP human joints respectively. The MCP joint is the metacarpal joint, i.e. the joint among the metacarpal phalange of the hand and the first phalanx of the finger, whereas the PIP (DIP) joint is the joint among the first (second) phalange and the second

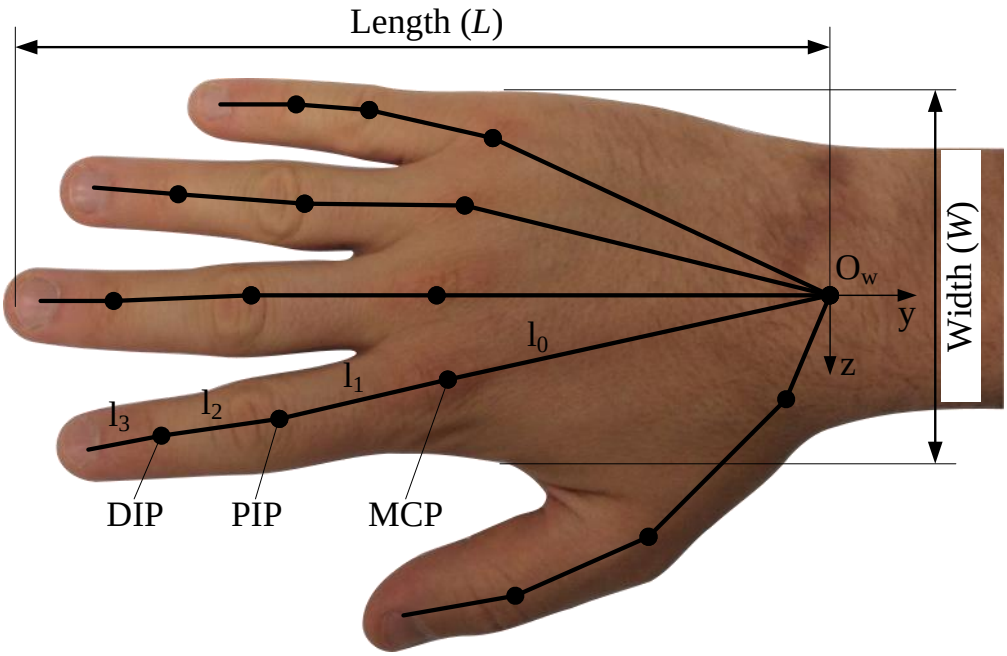

Figure 2.1 The hand model in Buchholz et al (1992).

Table 2.1 Average hand lengths (*L*) and hand width (*W*) of an European male, taken from Pheasant (2003).

Percentile	*L (mm)*	*W (mm)*
5^{th}	173	78
50^{th}	189	87
95^{th}	205	95

(third) phalange. See Appendix A for further details. With reference to Figure 2.1 (according to Buchholz et al, 1992) the length l_i, i = 0,..,3, of each finger phalanx and the position of each human joint (MCP, PIP and DIP) can be correlated to the length (*L*) and to the width (*W*) of the human hand. The position of each human joint (MCP, PIP and DIP) is given with respect to the system of coordinates (with axes x, y, z and origin O_w) fixed to the wrist, Figure 2.1. In Table 2.1 average values, taken from Pheasant (2003), of *L* and *W* of European males and corresponding to the 5^{th} percentile, 50^{th} percentile and 95^{th} percentile are reported. The hand model used in this Chapter for the grasping of a cylindrical object of diameter *d* is reported in Figure 2.2.

The model considers a planar motion of the human finger, neglects the abduction/adduction of the first phalange of the finger and considers the contact

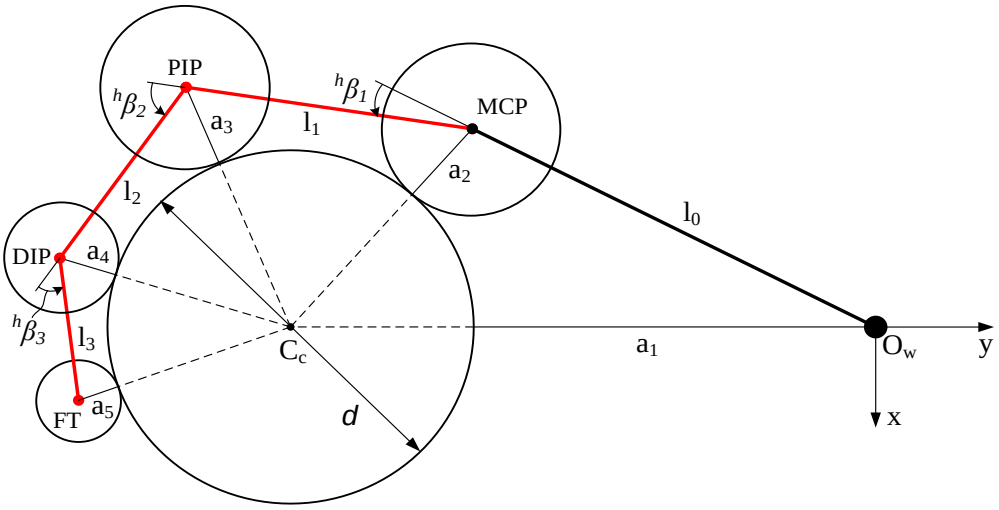

Figure 2.2 The hand model used.

Table 2.2. The anthropometric data measured. Measures reported in mm.

	a_1	a_2	a_3	a_4
m	70.9	17.3	12.5	27.3
sd	4.79	1.56	1.17	2.35

between the finger and the cylinder to grasp occurring at the MCP, PIP and DIP human joints and at the fingertip (Burton and Vaidyanathan, 2011). It provides the configuration of the human finger, i.e. the flexion angles ${}^h\beta_i$ (i = 1, 2, 3) where the superscript *h* refers to the hand model. The contact among the human joints and the cylinder to grasp is modelled as circles whose diameter coincides with the width of the human joint, placed in contact with the surface of the cylinder. With reference to Figure 2.2, a_1 is the distance from the centre of the wrist and the cylinder to grasp measured along the direction identified by the vector $\mathbf{O_wC_c}$, where C_c is the trace of the axis of the cylinder in the plane defined by the xy axis of the wrist, whereas a_i (i = 2,..,5) are the radii of the contact circles. According to Burton et al. (2011), the grasping model assumes $a_5 = a_4 / 2$ as a good approximation of the fingertip contact. To the author's knowledge, average measures of the human joints width are not reported in the literature. Thus, we measured the human joints of the index finger of ten people of average age of 32 years old. In Table 2.2, the mean values (*m*) and the standard deviation (*sd*) of the measured human joints are reported. We define as *slim finger,* a finger having the joints width a_i equal to $a_i = m - sd$, similarly we define as *medium finger* and *large finger* fingers having the joint widths equal to $a_i = m$ and $a_i = m + sd$ respectively.

2.2.2 The proposed mechanism for the finger guidance

The feasibility study of a planar 1-DoF mechanism, whose topology is conceived as suitable for all the fingers is the target of this first design step.
Some basic considerations for the synthesis of the targeted 1-DoF planar mechanism can be done, starting from the Grubler's formula for planar mechanisms:

Table 2.3. Mechanism topology to exploit 1-DoF planar motion with lower pairs.

n	4	6	8	10	12	…
c_1	4	7	10	13	16	…

$$l = 3(n-1) - 2c_1 - 2c_2 \tag{2.1}$$

where l is the number of DoFs of the mechanism, n is the number of links and c_1 and c_2 are the number of lower pairs (revolute and prismatic joints) and higher pairs (cam-follower type joints) respectively. Usually, cam-follower type joints are not adopted in hand exoskeletons for many reasons, e.g. complex design of a bilateral constraint, likelihood of high friction forces, etc. Considering mechanisms with lower pairs only and assuming $l = 1$, the mechanism topologies exploiting this features are reported in Table 2.3.

In this Chapter the focus is on the six-link mechanisms. Planar six-link mechanisms comprise seven links and six revolute joints and have two well-

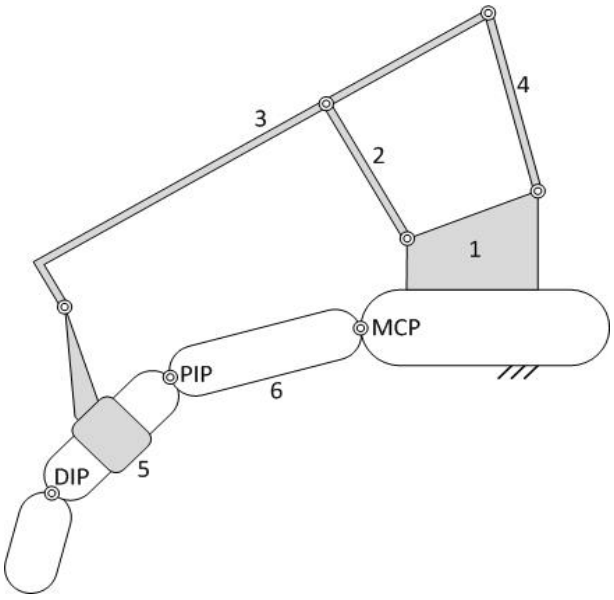

Figure 2.3 The finger exoskeleton based on a Stephenson III mechanism.

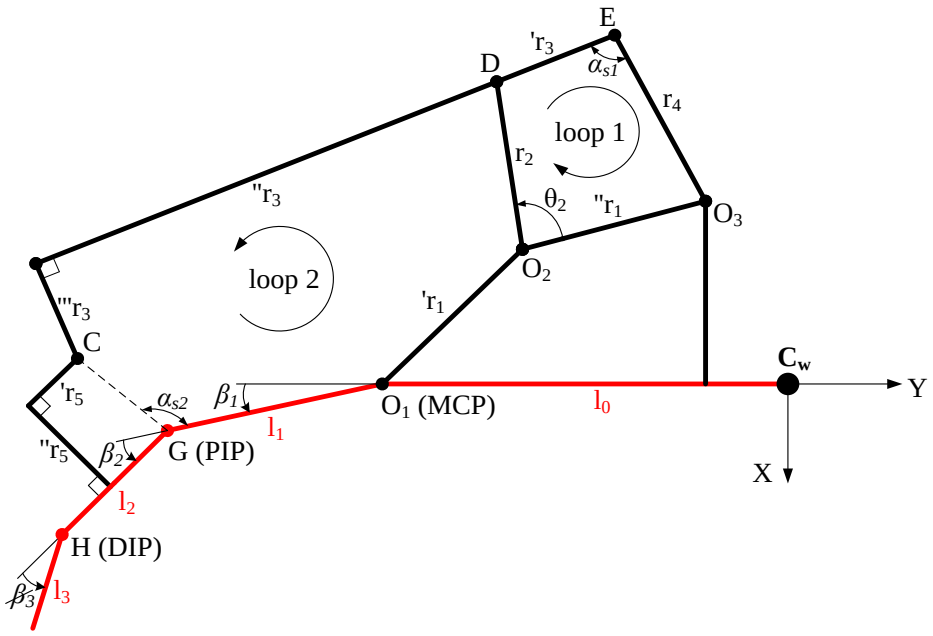

Figure 2.4 The Stephenson mechanism.

known topologically distinct configurations, called the Watt and the Stephenson six-bar chains.

Depending on which link is considered as the frame link, the Watt and the Stephenson chain yields to the Watt I, Watt II, Stephenson I, Stephenson II and Stephenson III linkages respectively. In this study, the Stephenson III mechanism was selected as a possible candidate for the motion guidance of the human finger. In Figure 2.3, the resulting exoskeleton based on this mechanism is reported. The first and the second phalanges are considered as parts of the mechanism, in particular link 5 of the mechanism comprises the second phalanx, whereas link 1 comprises the palm. The link 1 is the frame link, whereas link 2 is the moving link. The exoskeleton couples the flexion/extension movements of the first two phalanges through a number of poses (i.e., positions and orientations) corresponding to the grasp of a number of different cylindrical objects, and entails a natural motion of the finger along the grasping trajectory. The third phalange is free, i.e. its motion is not guided. The six-link mechanism is composed by two loops as shown in Figure 2.4.
The closure equations of the Stephenson mechanism are:

$$\begin{cases} \boldsymbol{O_2D} + \boldsymbol{DE} + \boldsymbol{EO_3} + \boldsymbol{O_3O_2} = \boldsymbol{0} \\ \boldsymbol{O_2D} + \boldsymbol{DC} + \boldsymbol{CG} + \boldsymbol{GO_1} + \boldsymbol{O_1O_2} = \boldsymbol{0} \end{cases} \tag{2.2}$$

By manipulating Equations (2.2), relationships between the phalanges configuration angles β_1, β_2 and the input angle θ_2 are obtained. These equations are not reported for the sake of conciseness. The mechanism singularity occurs when the links described by the vectors **CG** and $\mathbf{GO_1}$, and the links described by the vectors **DE** and $\mathbf{EO_3}$ are aligned. The synthesis problem here to tackle is to find the mechanism capable to guide the human phalanges so as they reach positions compatible with the selected power-grasping task while avoiding singularities of the mechanism during the grasping trajectory.

2.2.3 The dimensional synthesis

A numerical procedure is used to find a solution **x**, namely a vector containing the link lengths $'r_1$,$''r_1$, r_2, $'r_3$, $''r_3$, $'''r_3$, r_4, $'r_5$ *and* $''r_5$ by solving a constrained minimization problem specified as follows:

$$\min f_c(\boldsymbol{x}) \text{such that} \begin{cases} \boldsymbol{c}(\boldsymbol{x}) \le \boldsymbol{0} \\ \boldsymbol{l_b} \le \boldsymbol{x} \le \boldsymbol{u_b} \end{cases} \tag{2.3}$$

where the function $f_c(\mathbf{x})$, defined in details below, is the cost function that must be minimized; the vector $\boldsymbol{c}(\boldsymbol{x})$, also defined in details below, contains the constraints of the problem; the vectors $\boldsymbol{l_b}$ and $\boldsymbol{u_b}$ contain the lower and upper bounds of the solution vector **x**, respectively. The function $f_c(\mathbf{x})$ is defined as follows. Being the lengths l_i, i = 0,..,3, corresponding to the hand sizes reported in Table 2.1 and for a *medium finger* size of the finger, six finger configuration are considered. In particular five finger configurations corresponding to the grasp of five different cylindrical objects of diameters d, equals to 50, 60, 70, 80, 90 mm, respectively, and another configuration corresponding to the finger fully-extended are considered. For a generic vector **x** and considering a rotation of the moving angle θ_2 from 0 to 2π, the actual values ${}^a\beta_1$, ${}^a\beta_2$ are computed and the cost function is defined for each one of the six configurations for which ${}^a\beta_1 \equiv {}^h\beta_1$, thus the cost function $f_c(\mathbf{x})$ is:

$$f_c(\mathbf{x}) = \sum_{i=1}^{6} \frac{\left({}^{a}\beta_{2,i} - {}^{h}\beta_{2,i}\right)^2}{6} \tag{2.4}$$

where the index i = 1,..,6 refers to the six targeted finger configurations; the superscript a is referred to the actual mechanism; whereas the superscript h is referred to the hand grasping model. The vector $\boldsymbol{c}(\boldsymbol{x})$ is defined as:

$$\boldsymbol{c}(\boldsymbol{x}) = \begin{pmatrix} |\alpha_{s1} - \bar{\alpha}_{s1}| \\ |\alpha_{s2} - \bar{\alpha}_{s2}| \end{pmatrix} \tag{2.5}$$

where α_{sk}, k = 1,2, are the values of the angle between the two links described by the vectors **CG** and $\mathbf{GO_1}$ and the vectors **DE** and $\mathbf{EO_3}$ respectively, whereas $\bar{\alpha}_{sk}$ are the maximum threshold values of the angle α_{sk}. To keep $\boldsymbol{c}(\boldsymbol{x}) \leq \boldsymbol{0}$ means to avoid the mechanism singularities through all the desired trajectory. The optimization, performed by using a Genetic algorithm implemented in Matlab®, was done for the three hand lengths reported in Table 2.1, thus three different Stephenson mechanisms were found.

2.3 Simulations: result and discussions

Several simulations on the synthesized mechanism were conducted. The aim of the simulations is to evaluate the kinematic and the kinetostatic behaviour of the three exoskeletons found when they are used to guide the motion of a finger having a generic size. Considering a linear interpolation of the three hand sizes reported in Table 2.1 thirty one different hand sizes were extrapolated, moreover for each resulting hand size the index finger is considered to have *slim*, *medium* and *large* size, thus finally ninety three different index fingers are considered for these simulations. For the kinetostatic analysis of the mechanisms the force needed to grasp a cylinder is modeled as a force equal to F = 15 N applied in the middle of the second phalange and having direction perpendicular to the phalange itself. The counter torque M applied to the moving link 2 and the MCP and the PIP joint reaction forces, here called R_{MCP} and R_{PIP} respectively, are computed. The angular error e_i, i = 1,..,6, that occurred in reaching each of the six prescribed finger configurations is

Table 2.4. Results of the simulations.

Percentile	*5th*	*50th*	*95th*
W x L [mm]	173x78	189x87	205x95
e_{tot} *[°]*	29.2°	29.4°	17°
e_i *[°]*	8.3°	6.8°	3.6°
$max(R_{MCP},R_{PIP})$ *[N]*	13.8	15.6	28.5
satisfying test	6 / 93	9 / 93	3 / 93

computed. The error e_i is defined as $e_i = \left| {}^{a}\beta_{2,i} - {}^{h}\beta_{2,i} \right|$ for the configuration where ${}^{a}\beta_1 \equiv {}^{h}\beta_1$. Moreover, the total angular error e_{tot} in reaching all the six prescribed finger configurations is defined as $e_{tot} = \sum_{i=1}^{6} \left| {}^{a}\beta_{2,i} - {}^{h}\beta_{2,i} \right|$, where the index i (i = 1,..,6) refers to the six configurations that the finger must reach. Each one of the ninety three mechanisms tested is considered as useful for the motion guidance of the finger, if: each errors $e_i \leq 10°$, the error $e_{tot} \leq 30°$ (i.e. an average acceptable angular error of 5° for each one of the six configurations is admitted), and the maximum magnitude of the reaction forces R_{MCP} and R_{PIP} are less than 50 N. These thresholds were set by the authors as deemed common sense values.

Results of the simulations are summarized in Table 2.4, whereas in Figure 2.5 the total angular error e_{tot} is reported with respect to the different hand sizes considered.

The finger exoskeletons found by considering the hand size corresponding to the 5th, 50th and 95th percentile can be satisfactorily used for six, nine and three hands respectively. Results suggest that the synthesized finger exoskeletons can be used mainly for hand sizes close to the hand for which they are found.

However, the results are good considering that in general the mechanisms usually achieve good performances just for the reference task to which they are designed and small changes in the link lengths could provide low performances.

A 3D printed prototype of the finger exoskeleton was built, Figure 2.6. The link lengths of the prototype correspond to the link lengths of the mechanism found for a hand size corresponding to the 50th percentile.

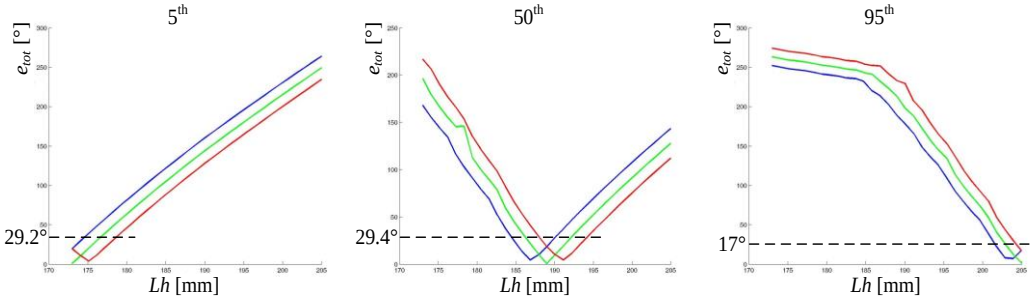

Figure 2.5 Errors e_{tot} for the different hand sizes tested. Blue lines refer to the *slim fingers*, green lines refer to the medium finger, whereas red lines refer to *large finger*.

Preliminary qualitative tests of such a prototype showed, as expected, a very good behaviour of the exoskeleton for hand sizes close to the 50th percentile.

In order to improve the number of hand sizes to which the exoskeleton can be fit, other simulations were conducted.

The possibility to use adjustable link length is investigated. In particular, interesting results were found by admitting to adjust the position of the revolute joint centered in the point C along a direction parallel to the second phalange (i.e. to adjust the length $'r_5$).

Results of the simulations, summarized in Table 2.5 and reported in Figure 2.7, showed that the finger exoskeletons found by considering the hand size corresponding to the 5th , 50th and 95th percentile can be satisfactorily used for twenty seven, forty five and fifteen hands respectively. Results showed that by admitting to adjust the link length $'r_5$, the synthesized finger exoskeletons can

Table 2.5 Results of the simulations for an adjustable length $'r_5$.

Percentile	*5th*	*50th*	*95th*
W x L [mm]	173x78	189x87	205x95
e_{tot} [°]	24.1°	23.2°	15.5°
e_i [°]	9.6°	9.6°	7.7°
max(R_{MCP},R_{PIP}) [N]	15.9	16	35.2
adjustable length [mm]	-1.2 ÷ 7.2	-5.6 ÷ 8	-3.7 ÷ 1
acceptable cases	27 / 93	45 / 93	15 / 93

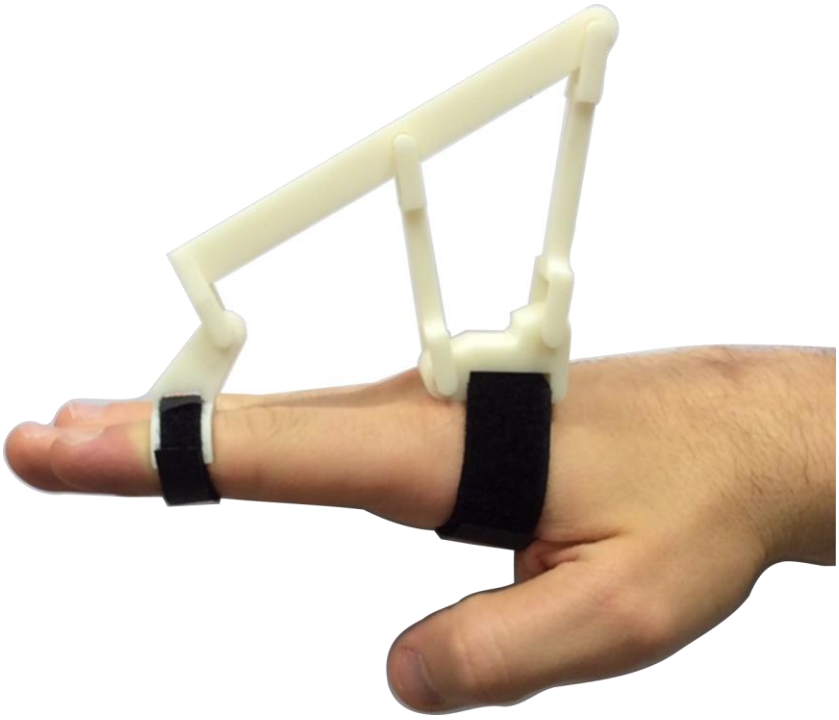

Figure 2.6 A 3D printed preliminary prototype of the proposed finger exoskeleton.

be used for an extend range of hand sizes, in particular the most interesting results are obtained for the mechanism corresponding to the 50th percentile hand sizes.

Finally, other four mechanisms to guide the motion of finger having size corresponding to the 50th percentile were synthesized and analysed. The results of the simulations are reported in Table 2.6 and revealed that a mechanism

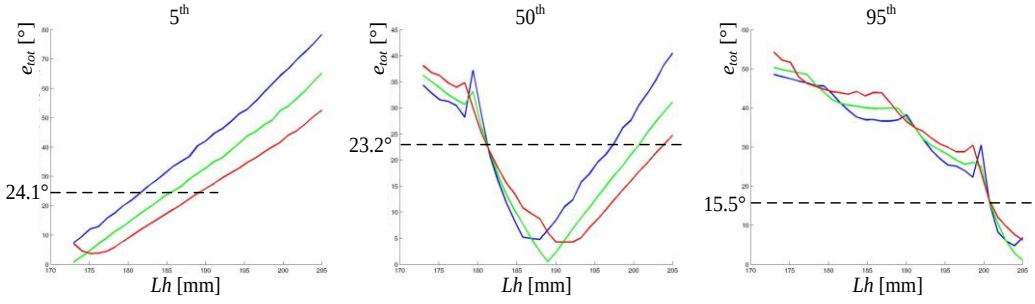

Figure 2.7. Errors e_{tot} for the different hand sizes tested considering as adjustable the position of the revolute joint identified by the point C. Blue lines refer to the *slim fingers*, green lines refer to the medium finger, whereas red lines refer to *large finger*.

Table 2.6 Results of the simulations considering the use of an adjustable link length.

Percentile	-	-	*50th*	-	-
W x L [mm]	186.6x85.8	187.9x86.4	189x87	190.06x87.5	191.1x88.06
e_i *[°]*	9.3°	9.9°	9.6°	9.5°	9.7°
e_{tot} *[°]*	27.7°	23.1°	23.2°	27.2°	25.1°
$max(R_{MCP},R_{PIP})$ *[N]*	14.5	17.9	16	23.2	17.1
adjustable length [mm]	-7 ÷ 7.8	-5.6 ÷ 6.9	-5.6 ÷ 8	-4.2 ÷ 7.3	-5.5 ÷ 4.5
acceptable cases	51 / 93	48 / 93	45 / 93	42 / 93	45 / 93

designed for an hand having L = 187.9 mm and W = 86.4 mm could be satisfactorily used on a large number of hands by admitting a reasonable variability of the link r_5'.

Chapter 3

Dimensional synthesis of the RSSR mechanism for the optimal transmission of motion and forces to the thumb mechanism

3.1 Introduction

Recently, our research group built a new hand exoskeleton called Bologna Hand Orthoses (BHO) for the robotic rehabilitation of post-stroke patients. In Chapter 1, the design specifications that guided the overall project in addition to a brief description of the final prototype were reported. Moreover, some considerations on the final prototype were discussed with the aim to highlight some challenging problems to be solved for a future version of the device. Particularly interesting for the aim of this Chapter is the problem regarding the motion transmission to the thumb.

The design philosophy adopted to build the BHO, is to keep fix the first phalange of the thumb, and to guide the flexion/extension motion of both the second and third phalanges only. In particular, the flexion/extension of the thumb is guided by a planar mechanism placed above the finger; the mechanism comprises 8 links and 11 revolute joints, and both the human phalanges and the anatomical articulations are part of the mechanism. Generally speaking, to fix the pose of the first phalange of the thumb means to fix the plane of motion of the thumb with respect to the four fingers. Thus, for the BHO, the plane of motion of the thumb mechanism doesn’t change during the flexion/extension

motion-in-operation of the thumb. The therapist, during the fitting procedure of the BHO to the patient hand, must choose the appropriate pose of the first phalange of the thumb, namely the appropriate pose of the plane of motion of the thumb mechanism, according to the natural patient hand anthropometric geometry. In order to choose the best plane of motion, a passive mechanism (i.e. a mechanism with passive joints) was used (see Chapter 1 for further details). The passive mechanism comprises four revolute and two prismatic joints, thus it is a 4R2P mechanism. The configuration of the 4R2P passive mechanism can be manually adjusted and fixed during the fitting procedure of the hand exoskeleton to the patient hand. The motion is transmitted from the DC motor to the moving link of the thumb mechanism by the use of a RSSR mechanism. The frame link of the RSSR mechanism coincides with the 4R2P mechanism. As a result, since the geometry of the 4R2P passive mechanism must be regulated during the fitting procedure, the frame link of the RSSR consequently changes. In general, to change the geometry of a mechanism means to change its performances in terms of motion and force transmission characteristics; in order to avoid this problem, the link length of the coupler link of the RSSR mechanism used in the BHO (i.e. the connecting rod between the two spherical joints) can be ad hoc regulated in order to provide the optimal motion and force transmissibility for different patients. However, from the practical point of view, it results quite difficult to properly set the link length of the coupler link, with the risk, in general, that the motion and force transmission characteristics of the RSSR mechanism move away from the optimal operating conditions. A possible improvement of the existing solution can be obtained by simplifying the fitting procedure. Given this interest, the idea is to avoid the adaptability of the coupler link of the RSSR mechanism, thus defining a new RSSR mechanism capable to transmit as-best the motion and forces to the thumb mechanism for a given range of frame link geometries (thus corresponding to different hand patient geometries).

This Chapter deals with the dimensional synthesis of a RSSR mechanism characterized by having fixed link lengths of the floating links, while ensuring the optimal motion and force transmission characteristics for different frame link geometries. The synthesis procedure is firstly presented in a general way, and then applied to the BHO hand exoskeleton.

3.2 The RSSR mechanism

3.2.1 State of the art of the RSSR mechanism synthesis

The RSSR mechanism is one of the most popular mechanisms typically used to transmit motion and forces between two shafts with skew axes (called input and output axes hereinafter).

The synthesis of the RSSR mechanism for the optimal rotatability and/or optimal transmission of motion and forces has been extensively studied in the literature, and different synthesis procedures have been proposed. Since the optimization of the force transmission guarantees a better functioning of the mechanism (Balli and Chand, 2002), many authors presented original synthesis procedures exploiting the definition of indices whose measure assesses both the quality of motion and force transmission (Balli and Chand, 2002; Sutherland and Roth, 1973; Sutherland, 1981; Tsai and Lee, 1994; Chen and Angeles, 2007). Remarkable works deal with the mobility analysis of the RSSR mechanism (Nolle, 1969; Kazerounian and Solecki, 1993), the synthesis of fully rotatable RSSR linkage with transmission angle control (Gupta and Kazerounian, 1983; Alizade and Sandor, 1985; Rastegar and Tu, 1992; Soylu and Kanberoglu, 1993), the transmission optimization of the RSSR mechanism with a given rocker swing angle, a corresponding crank rotation and the optimum force transmission (Söylemez and Freudenstein, 1982; Söylemez, 1993; Soylu, 1993), the optimum path generation synthesis (Alizade et al., 1976; Sancibrian et al., 2007), the synthesis based on a given time ratio (Balaji Rao and Lakshminarayana, 1984), and the RSSR mechanism with partially constant transmission angle (Şaka, 1996). As regards the measure of both the quality of motion and force transmission of mechanisms, several indices are available in the literature. An extended literature review is reported by Balli and Chand (2002). Sutherland and Roth (1973) introduced the Transmission Index (*TI*) as an indicator of the quality of motion transmission for single loop spatial mechanisms. The value of *TI* depends only on both mechanism geometry and configuration, whereas no information on forces and torques acting on each

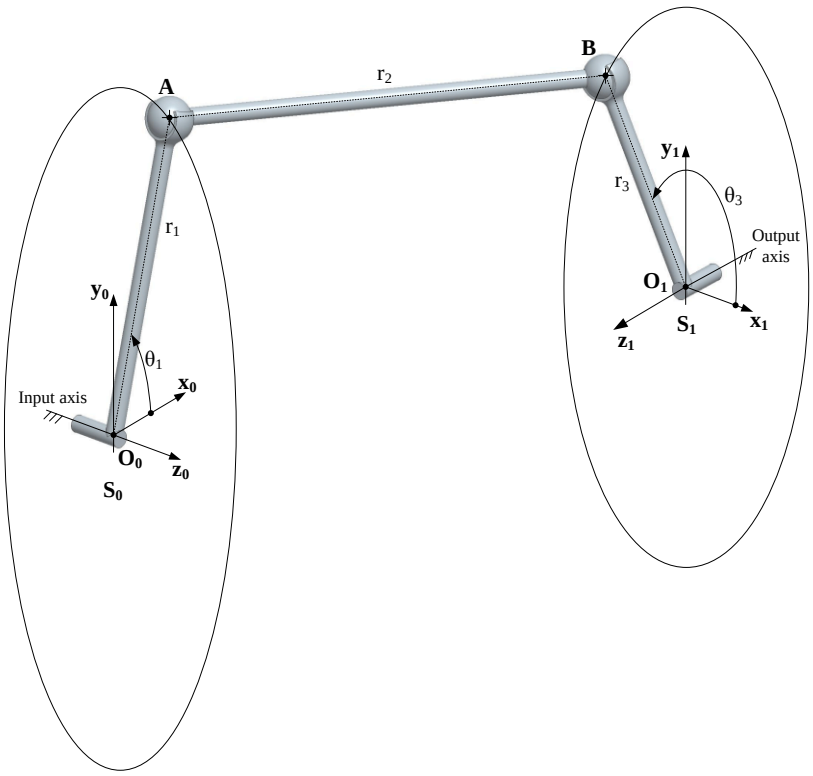

Figure 3.1 The RSSR spatial mechanism.

joint is required to define *TI*. However, optimizing *TI* means maximizing the mechanism performances of both motion and force transmission (Sutherland and Roth, 1973; Sutherland, 1981).

3.2.2 Basic kinematic equations

The spatial RSSR mechanism has four binary links: the driving link is coupled to the frame and to the coupler through a revolute and a spherical pair respectively; the coupler is then connected to the follower by a spherical pair, and the follower is connected to the frame through a revolute pair. Disregarding the rotation of the coupler about the axis defined by the two spherical pair centres, the mechanism has one degree of freedom. It converts a rotation about one axis into a rotation about a second axis, generally skew in space, with a variable transmission ratio. Depending on the link geometry, the linkage can be of three types: drag-link, crank-and-rocker or double-rocker (see Nolle, 1969 for further details).

For any given frame link geometry, the parameters needed to define the

mechanism geometry, the transmission ratio τ and the Transmission Index *TI* are reported below.

With reference to Figure 3.1, two right hand Cartesian coordinate systems S_0 (with axes x_0, y_0 and z_0 and origin O_0) and S_1 (with axes x_1, y_1 and z_1 and origin O_1) fixed to the frame of the RSSR mechanism are defined. The axis z_0 of S_0 coincides with the input axis of the RSSR mechanism, whereas the axis z_1 of S_1 coincides with the output axis of the mechanism. The axes x_0, y_0 and x_1, y_1 are arbitrarily oriented. The origin O_0 (O_1) of S_0 (S_1) is on the intersection of the input (output) axis with the plane containing the centre A (B) of the spherical joint and orthogonal to the input (output) axis. The relative pose of S_1 with respect to S_0 is given by a 4x4 matrix M_{01}, generally written in the form:

$$M_{01} = \begin{pmatrix} \mathbf{S_{01}} & {}^0(\mathbf{O_1} - \mathbf{O_0}) \\ 0 & 1 \end{pmatrix} = \begin{pmatrix} s_{11} & s_{12} & s_{13} & x_{01} \\ s_{21} & s_{22} & s_{23} & y_{01} \\ s_{31} & s_{32} & s_{33} & z_{01} \\ 0 & 0 & 0 & 1 \end{pmatrix} \tag{3.1}$$

where the 3x1 vector ${}^0(\mathbf{O_1} - \mathbf{O_0})$ collects the coordinates $(x_{01}\ y_{01}\ z_{01})$ of the origin O_1 measured in S_0, whereas the 3x3 matrix $\mathbf{S_{01}}$ represents the relative orientation of S_1 with respect to S_0. A well-known parameterization of the 3x3 matrix $\mathbf{S_{01}}$ makes use of the three Euler angles. In this Chapter, the angles β_z, β_y and β_x are the Euler angles corresponding to three rotations performed about the moving axes z, y, x, respectively, to move S_1 from S_0 to its actual orientation.

The moving link lengths are defined as follows:

- $r_1 = |(\mathbf{A} - \mathbf{O_0})|$, driving link (link 1) length, i.e. the distance of point A from the input axis;
- $r_2 = |(\mathbf{B} - \mathbf{A})|$, coupler link (link 2) length, i.e. the distance between points A and B;
- $r_3 = |(\mathbf{B} - \mathbf{O_1})|$, follower link (link 3) length, i.e. the distance of point B from the output axis;

The input and output link angles are defined as follows:

- θ_1, input link angle measured about z_0 according to the right-hand rule from the axis x_0 to the vector $(\mathbf{A} - \mathbf{O_0})$;

- θ_3, output link angle measured about z_1 according to the right-hand rule from the axis x_1 to the vector (**B - O_1**).

The equation that relates the rotation of the input and output shafts of the RSSR mechanism can be obtained by the following constraint equation:

$$(\mathbf{A}-\mathbf{B})^T \cdot (\mathbf{A}-\mathbf{B}) - r_2^{\,2} = 0 \tag{3.2}$$

Expanding (3.2) and rearranging the terms leads to the mechanism displacement equation:

$$d\cos\theta_3 + e\sin\theta_3 = f \tag{3.3}$$

where

$$d = 2r_3 s_{11}(x_{01} - r_1\cos\theta_1) + 2s_{21}(y_{01}r_3 - r_1 r_3 \sin\theta_1) + 2r_3 s_{31} z_{01}$$
$$e = 2r_3 s_{12}(x_{01} - r_1\cos\theta_1) + 2r_3 s_{22}(y_{01} - r_1\sin\theta_1) + 2r_3 s_{32} z_{01}$$
$$f = r_2^{\,2} - r_3^{\,2} - z_{01}^{\,2} - y_{01}^{\,2} - z_{01}^{\,2} - r_1^{\,2} + 2r_1 x_{01}\cos\theta_1 + 2y_{01} r_1 \sin\theta_1$$

By substituting trigonometric identities into the general displacement equation (3), the relationship between θ_1 and θ_3 is:

$$\theta_3 = \operatorname{atan}\left(\frac{e}{d}\right) \pm \operatorname{acos}\left(\frac{f}{\sqrt{d^2+e^2}}\right) \tag{3.4}$$

The plus or minus sign refers to the two different modes to assemble an RSSR mechanism for a given θ_1.

The transmission ratio τ, defined as the ratio between the angular velocities $\dot{\theta}_3$ and $\dot{\theta}_1$ of the output and input shafts respectively, is given by:

$$\tau = \frac{\dot{\theta}_3}{\dot{\theta}_1} = \frac{d'\cos\theta_3 + e'\sin\theta_3 - f'}{d\sin\theta_3 - e\cos\theta_3} \tag{3.5}$$

where

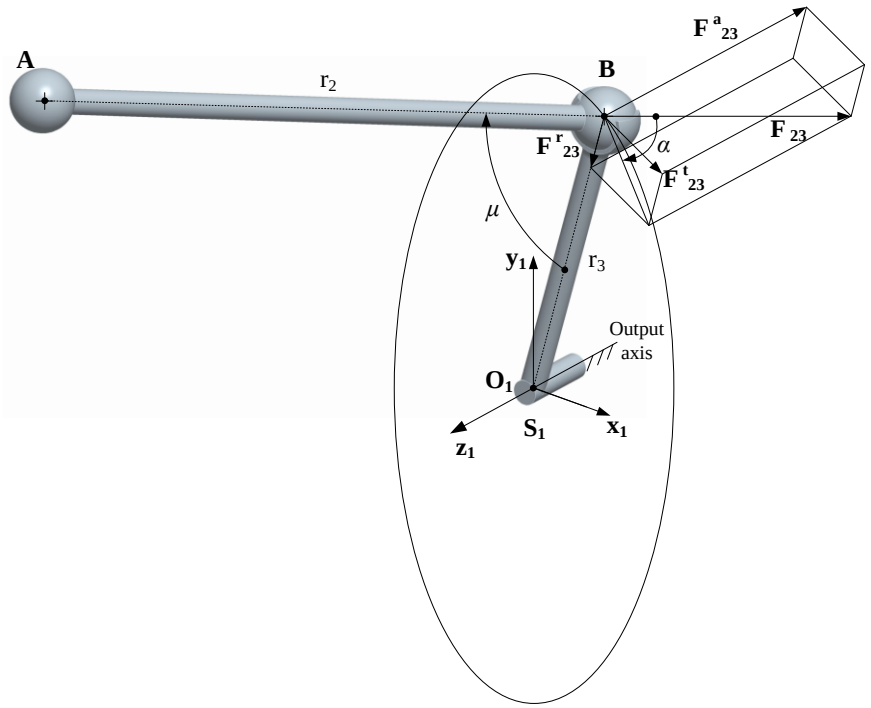

Figure 3.2 Force transmission between the coupler and the output link of the RSSR mechanism.

$$d' = \frac{\partial d}{\partial \theta_1} = 2r_3 s_{11} r_1 \sin\theta_1 - 2r_1 r_3 s_{21} \cos\theta_1$$

$$e' = \frac{\partial e}{\partial \theta_1} = 2r_1 r_3 s_{12} \sin\theta_1 - 2r_1 r_3 s_{22} \cos\theta_1$$

$$f' = \frac{\partial f}{\partial \theta_1} = -2r_1 x_{01} \sin\theta_1 + 2r_1 y_{01} \cos\theta_1$$

According to the definition of *TI* given by Söylemez and Freudenstein (1982) and referring to Figure 3.2, the Transmission Index *TI* of a linkage can be expressed as:

$$TI = \frac{\left|\mathbf{F}_{23}^{\mathbf{t}}\right|}{\left|\mathbf{F}_{23}\right|} = \sqrt{1 - \cos^2\mu - \sin^2\alpha} \tag{3.6}$$

where,

$$\cos\mu = \frac{1}{2}\frac{1}{r_2 r_3}\left(r_2^{\,2} + r_3^{\,2} - \left(r_1^{\,2} + x_{01}^{\,2} + y_{01}^{\,2} + z_{01}^{\,2} - 2r_1 x_{01}\cos\theta_1 - 2r_1 y_{01}\sin\theta_1\right)\right)$$

$$\sin\alpha = r_1\left(s_{13}\cos\theta_1 + s_{23}\sin\theta_1\right) - \left(s_{13}x_{01} + s_{23}y_{01} + s_{33}z_{01}\right)$$

$\mathbf{F_{23}}$ is the force exerted on the output link by the coupler that, ignoring friction, has the direction of the vector (**B - A**). The force $\mathbf{F_{23}}$ can be decomposed into three orthogonal components $\mathbf{F_{23}^r}$, $\mathbf{F_{23}^a}$ and $\mathbf{F_{23}^t}$. $\mathbf{F_{23}^r}$ is the force component exerted on the radial direction defined by the vector (**B - O$_1$**), $\mathbf{F_{23}^a}$ is the axial force component exerted on the direction of the output axis, while $\mathbf{F_{23}^t}$ is the force component in the plane orthogonal to the output axis and tangent to the trajectory of point B. The forces $\mathbf{F_{23}^r}$ and $\mathbf{F_{23}^a}$ do not produce torque on the output shaft, whereas $\mathbf{F_{23}^t}$ is responsible for the output torque. Angle μ is the angle between vectors (**B - A**) and (**B - O$_1$**), angle α is the angle between $\mathbf{F_{23}^t}$ and the resultant of $\mathbf{F_{23}^t}$ and $\mathbf{F_{23}^r}$. The Transmission Index, variable between 0 and 1, generally depends on the mechanism configuration, i.e. it is a function of the driving link angle θ_1. A linkage configuration for which *TI* = 1 has the optimum force and motion transmission performances (Sutherland and Roth, 1973).

3.3 The proposed synthesis procedure

To univocally describe the geometry of the RSSR mechanism, a set $\mathbf{U_1}$ of *n* geometry parameters is necessary. Let the set $\mathbf{U_1}$ be split into two subsets, $\mathbf{U_2}$ and $\mathbf{U_3}$, comprising *m* (*m*<*n*) and (*n*–*m*) of the *n* geometry parameters respectively ($\mathbf{U_2} \cup \mathbf{U_3} = \mathbf{U_1}$ and $\mathbf{U_2} \cap \mathbf{U_3} = \varnothing, \mathbf{U_2} \subset \mathbf{U_1}$). The elements of the sets $\mathbf{U_2}$ and $\mathbf{U_3}$ are here called design parameters and design variables respectively. The design parameters are usually considered as univocally assigned in the above mentioned synthesis problems, whereas the design variables are determined by the synthesis procedures. For example, in Söylemez and Freudenstein (1982), the design parameters are the parameters

corresponding to the frame link geometry, whereas the design variables are the moving link lengths of the resulting RSSR mechanism. A different problem can be considered if each element $u_{2,i}$, $i=1,..,m$, of the set $\mathbf{U_2}$ is required to vary within a given range of values (bounded between the values $\bar{u}_{2,i}$ and $\tilde{u}_{2,i}$) rather than being assigned as a single value, thus m sets $\mathbf{U_{2,i}} = \left\{ u_{2,i} \mid u_{2,i} \in \left[\bar{u}_{2,i}, \tilde{u}_{2,i} \right] \right\}$, $i=1,..,m$, are consequently defined. This represents a new synthesis problem. In general, varying a design parameter means obtaining a different mechanism which has different functional performances as a consequence. Therefore imposing the m sets $\mathbf{U_{2,i}}$ of the design parameters means obtaining an infinite number of $\mathbf{U_3}$ sets of the design variables, i.e. obtaining a set of different mechanisms which have again different functional performances as a consequence. The synthesis problem here tackled is to impose the sets $\mathbf{U_{2,i}}$, $i=1,..,m$, of the design parameters and find the set of design variables that optimizes some objective function while satisfying at the same time constraints and technical specifications given by the designer, according to the problem under study. To guarantee the optimal force transmission performance for the resulting mechanism, the Transmission Index *TI* is here taken as the objective function. The particular synthesis problem here tackled is to find the design variables of the RSSR mechanism, aiming at the optimization of the force transmission, while satisfying the following constraints: definition of the design parameters and determination of the m sets $\mathbf{U_{2,i}}$, prescription of the extreme angular position values for both the input and the output links, prescription of the upper and lower bounds of the transmission ratio and prescription of the upper and lower bounds of the value of the design variables.

In the author's opinion, an efficient solution of this problem is far from being straightforward, and an analytical solution of the problem is not feasible in general.

3.3.1 The algorithm

The problem is to find the design variables, i.e. to synthesize an RSSR

mechanism for m given sets $\mathbf{U}_{2,i}$ of the design parameters ($i=1,..,m$), where the design parameters are chosen as the six independent parameters x_{01}, y_{01}, z_{01}, β_x, β_y, β_z needed to define the 4x4 matrix M_{01} (hence m = 6). Each design parameter is here considered as variable within a given range of values. The design variables are the three link lengths r_1, r_2 and r_3 of the moving links. As regards the input (output) link, the initial position angle θ_{10} (θ_{30}) and the swing angle $\Delta\theta_1$ ($\Delta\theta_3$) are assigned by the designer. In addition, since severe constraints for this synthesis problem are imposed, tolerances on the reaching of the extreme position values for the output link are admitted. In particular, the angular position maximum errors ε_1 and ε_2 on the initial position angle θ_{30}, and on the swing angle $\Delta\theta_3$ respectively, are set by the designer. Similarly, the upper and lower bounds (τ_{MIN},τ_{MAX}) for the transmission ratio values are assigned by the designer.

The aim of this study is the dimensional synthesis of the moving links of an RSSR mechanism, taking the optimization of the force transmission as the objective function, while respecting prescribed constraints (*i*) on the m given sets $\mathbf{U}_{2,i}$ of the design parameters, (*ii*) on given angular position values for the input link, (*iii*) on given angular position values, and relative angular position maximum errors, for the output link, (*iv*) on the upper and lower limits for the transmission ratio, and finally (*v*) on the upper and lower limits for the value of the design variables of the resulting RSSR mechanism.

A numerical procedure is used to find a solution **x**, namely a vector containing the three link lengths r_1, r_2 and r_3, by solving a constrained minimization problem. From the given m sets $\mathbf{U}_{2,i}$, N different sets $\mathbf{V}_k$, $k=1,..,N$, $\mathbf{V}_k=\{u_{2,i}\,|\,u_{2,i}\in\mathbf{U}_{2,i}, i=1,..,m\}$ are selected by the designer according to the specific application studied. The constrained minimization problem is specified as follows:

$$\min_x f_c(\mathbf{x}) \text{ such that } \begin{cases} \mathbf{c}_k(\mathbf{x})\le\mathbf{0} \quad \forall\ k=1,..,N \\ \mathbf{l_b}\le\mathbf{x}\le\mathbf{u_b} \end{cases} \tag{3.7}$$

where the function $f_c(\mathbf{x})$, defined in detail below, is the cost function returning a scalar that must be minimized; the vectors $\mathbf{c}_k(\mathbf{x})$, also defined in detail

below, are the constraint vectors, i.e. they are vectors whose components represent the constraints; the vectors $\mathbf{l_b} = \begin{bmatrix} r_{1min} & r_{2min} & r_{3min} \end{bmatrix}$ and $\mathbf{u_b} = \begin{bmatrix} r_{1max} & r_{2max} & r_{3max} \end{bmatrix}$ contain the lower and upper bounds of the solution vector **x**, respectively.

The cost function $f_c(\mathbf{x})$ and the constraint vectors $\mathbf{c}_k(\mathbf{x})$ are defined as follows: for a generic vector **x** and for each $\mathbf{V}_k$ ($k = 1,..,N$), considering a rotation of the driving link angle from θ_{10} to $\theta_{10} + \Delta\theta_1$, the algorithm computes the values of the output link angle θ_3, the transmission ratio τ, and the Transmission Index *TI*. The cost function $f_c(\mathbf{x})$ is defined as:

$$f_c(\mathbf{x}) = \left(\sum_{k=1}^{N} \left(max\left(1 - TI_k\right)\right)^p \right)^{1/p} \tag{3.8}$$

where the term $\max(1\text{-}TI_k)$ is the maximum value of the complement to 1 of the Transmission Index, i.e. it represents the worst case in terms of motion transmission among the mechanism configurations. The scalar $p\ (\geq 1)$ can be set by the designer to emphasize the largest values of $max(1 - TI_k)$. The constraint vectors $\mathbf{c}_k(\mathbf{x})$ are defined as:

$$\mathbf{c}_k(\mathbf{x}) = \begin{pmatrix} \left|\theta_{30,k} - \theta_{30}\right| - \varepsilon_1 \\ \left|\Delta\theta_{3,k} - \Delta\theta_3\right| - \varepsilon_2 \\ max(\tau_k) - \tau_{MAX} \\ \tau_{MIN} - min(\tau_k) \end{pmatrix} \tag{3.9}$$

where $\theta_{30,i}$ and θ_{30} are the actual and the reference initial position angles respectively, $\Delta\theta_{3,k}$ and $\Delta\theta_3$ are the actual and the reference swing angles respectively, and finally $max(\tau_k)$ and $min(\tau_k)$ are the maximum and minimum values for the transmission ratio τ respectively.

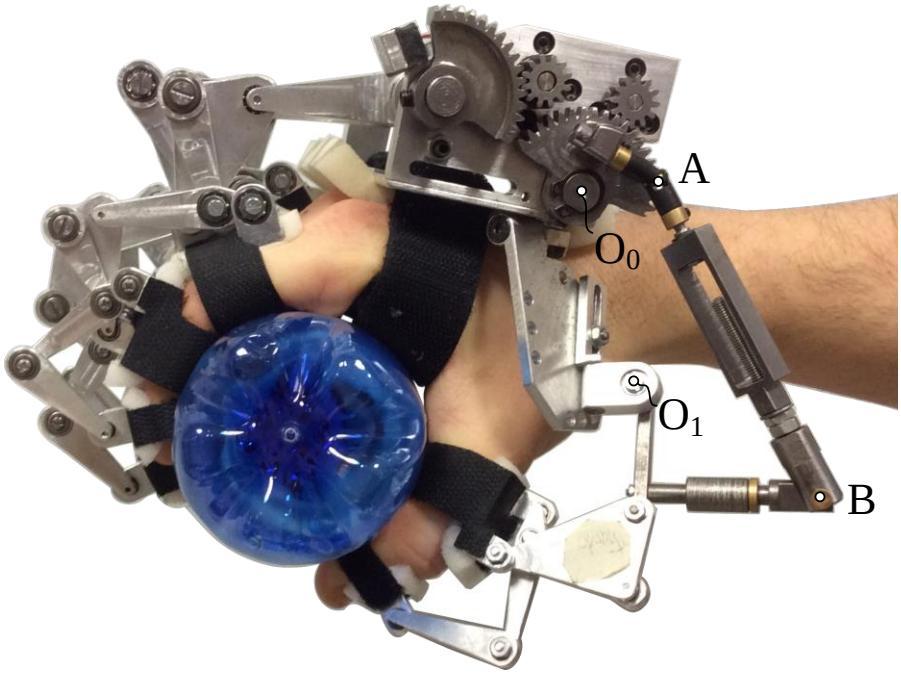

Figure 3.3 The BHO hand exoskeleton.

The optimization is performed by solving the minimization problem represented in Equation (3.7) in two steps, by using firstly a Genetic algorithm (the Matlab® function `ga`), the solution is then refined by means of a quasi-Newton algorithm (the Matlab® function `fmincon`). Once the algorithm convergence is achieved, the optimization finds the solution vector $\tilde{\mathbf{x}} = \left[\tilde{r}_1 \quad \tilde{r}_2 \quad \tilde{r}_3\right]$ that minimizes the values of $f_c(\mathbf{x})$ and satisfies the imposed constraints, i.e. $\mathbf{c}_k(\mathbf{x}) \le 0 \quad \forall\, k = 1,..,N$.

3.4 Application of the synthesis procedure to the BHO

The optimization algorithm is implemented and tested in a case study coming from the problem of designing an RSSR mechanism selected for the transmission of motion to the thumb of the BHO. With reference to Figure 3.1 and Figure 3.2, the points A and B are the centres of the two spherical pairs, whereas the points O_0 and O_1 belong to the frame link of the RSSR mechanism.

As explained in Chapter 1, the moving link of the RSSR mechanism is rigidly connected to the actuator (that is fastened to the hand backside) whereas

the output shaft is rigidly connected to the driving link of the thumb mechanism (that is fastened to the metacarpal bone of the thumb). In this perspective, the six design parameters that describe the relative pose of the two shafts are strictly related to the patient's anatomical geometry. For different patients the design parameters thus vary in certain ranges, corresponding to different frame link geometries of the RSSR mechanism. The synthesis task is therefore to find the design variables that provide the optimal transmission of torque for all patients. In the implementation of the problem, the thumb exoskeleton is fitted on a reference patient with a hand length of 190 mm and a hand width of 90 mm. The hand length is measured from the distal crease of the wrist to the middle finger tip, whereas the hand width is measured across the back of the hand from the MCP joint of the index finger to the MCP joint of the little finger. The finger bones' lengths are related to the hand length and width by means of coefficients proposed by Buchholz et al. (1992). The values of the design parameters are:

- $^{0}\left(\mathbf{O}_1-\mathbf{O}_0\right)^{ref}=\left(x_{01}^{ref}\quad y_{01}^{ref}\quad z_{01}^{ref}\right)^T=\left(26.83\quad -65.92\quad -12.08\right)^T$ mm
- $\left(\beta_x^{ref}\quad \beta_y^{ref}\quad \beta_z^{ref}\right)=\left(35.0°\quad -10.5°\quad -115.5°\right)$

where superscript *ref* refers to the reference patient.

The need to fit the exoskeleton to different patient hands is taken into account by assuming that the origin O_1 of the reference system S_1 may vary in a cube of side $\delta_1=5\,\text{mm}$ and centred in $^{0}\left(\mathbf{O}_1-\mathbf{O}_0\right)^{ref}$, thus $x_{01}=x_{01}^{ref}\pm\delta_1/2$, $y_{01}=y_{01}^{ref}\pm\delta_1/2$ and $z_{01}=z_{01}^{ref}\pm\delta_1/2$. The side of the cube is discretized in $q_1=2$ discrete values. As regards the orientation, for each new origin O_1, $q_2=2$ discrete values of a rotation $\delta_2=10°$ of the system S_1 about its axis x_1 are considered. The rotations are taken as $\beta_x=\beta_x^{ref}\pm\delta_2/2$, $\beta_y=\beta_y^{ref}$ and $\beta_z=\beta_z^{ref}$. Therefore $N=81$ sets $\mathbf{V}_k$ are selected. The variable θ_1 associated with the input link position is discretized in 360 values with a 1 degree step. The values of the other parameters are reported in Table 3.1.

The sizes of the links are bounded within the following ranges:

Table 3.1 Numerical values of the input parameters.

θ_{10}	$\Delta\theta_1$	$\theta_{30} \pm \varepsilon$	$\Delta\theta_3 \pm \varepsilon_2$	τ_{MIN}	τ_{MAX}	p
0	90°	90° ± 9°	45° ± 4.5°	0	1	3

- $20 \le r_1 \le 100$
- $40 \le r_2 \le 130$
- $20 \le r_3 \le 100$

where the values are given in mm.

3.5 Results and discussions

The algorithm requires a computational time of about 70 s in a personal computer with standard performance (Intel(R) Core(TM) i3-2120 CPU @ 3.3 GHz) and provides the results reported in Table 3.2.

A second run with $q_1 = 4$ and $q_2 = 4$ is done, thus $N = 625$ sets $\mathbf{V}_k$ are selected. The algorithm requires a computational time of about 490 s and finds exactly the same solution previously obtained. The aim of this successive run is to check the reliability of the solution previously found. The value of $\delta_1 = 5\,\text{mm}$ and $\delta_2 = 10°$ are small with respect to the dimension of the whole mechanism; however, because of the severe constraints imposed by the practical problem the solution does not exist for greater values of δ_1 and δ_2. For example, the algorithm does not find any solution for the values of $\delta_1 = 10\,\text{mm}$ and $\delta_2 = 10°$.

The solution found for the values of $\delta_1 = 5\,\text{mm}$ and $\delta_2 = 10°$ is quite good in terms of motion characteristics, considering that $\text{TI}_{\min} = \min_k \left(TI_k \right) = 0.482$ ($k = 1,..,N$), thus meaning that in the worst case about 48.2% of the amplitude

Table 3.2. Results of the simulation.

$f_c(x)$	r_1 [mm]	r_2 [mm]	r_3 [mm]
2.05	26.73	107.02	74.08

Table 3.3 Percentage of frame link poses, $e_{\%}$, and mean values $\mathrm{TI}_{\mathrm{mean}}$, corresponding to given minimum values of $\mathrm{TI}_{\mathrm{min}}$ to be achieved.

$\mathrm{TI}_{\mathrm{min}}$	0.49	0.50	0.51	0.52	0.53	0.54	0.55	0.56
$e_{\%}$	98.56%	89.60%	74.72%	59.04%	43.36%	28.16%	12.96%	2.080%
$\mathrm{TI}_{\mathrm{mean}}$	0.653	0.656	0.660	0.663	0.668	0.672	0.678	0.688

of the force transmitted from the coupler to the output shaft is usefully exploited to produce torque. The mean value of *TI* is, $\mathrm{TI}_{\mathrm{mean}} = \underset{k}{\mathrm{mean}}\left(TI_k\right) = 0.653$ which is rather a good performance. However, some applications could require $\mathrm{TI}_{\mathrm{min}}$ to be larger than a minimum threshold. If $\mathrm{TI}_{\mathrm{min}}$ is not satisfactory, some options can be considered:

1) accept having a satisfactory solution only in a limited percentage of the whole frame link geometries. For instance, by referring to the presented results with $N = 625$, Table 3.3 reports the percentage $e_{\%}$ of the 625 poses corresponding to the achievement of certain minimum values of $\mathrm{TI}_{\mathrm{min}}$; the corresponding mean value $\mathrm{TI}_{\mathrm{mean}}$ is also reported. Results show that, for instance, if $\mathrm{TI}_{\mathrm{min}} = 0.49$ is the minimum threshold, 98.56% of the 625 poses satisfies the requirement, with a corresponding mean value of $\mathrm{TI}_{\mathrm{mean}} = 0.653$. If higher values are required, the percentage rapidly decreases: for required values of $\mathrm{TI}_{\mathrm{min}}$ greater than 0.56, the percentage of acceptable mechanisms reaches minimum levels.

2) Change the problem by admitting the use of adjustable mechanisms in order to obtain an acceptable value for $\mathrm{TI}_{\mathrm{min}}$. The adjustable mechanisms have one or more links (typically the coupler link) with variable geometry. It is worth noting that the use of adjustable mechanisms does not increase the complexity of the problem. Indeed, the possibility to adjust, for example, the length of the coupler link when moving from one frame link geometry to another one can be considered as a new problem with the constraints more relaxed than in the problem investigated here. If all three lengths r_1, r_2 and r_3 are assumed as adjustable, the problem would be to find an RSSR mechanism for each different

set $\mathbf{V}_k$.

It is worth noting that to verify the stability of the solution different runs were performed by changing the setup parameters of the algorithm (e.g. the number of discrete values for the input angle θ_1, the number of generations and the initial population of the *ga*, etc.). The reliability of the numerical procedure is confirmed by the same results obtained for the different runs.

Chapter 4

Experimental measures and analysis of the spatial motion of the human fingers

4.1 Introduction

The aim of this Chapter is to measure and analyse the spatial motion of the human fingers. It was decided to put this Chapter at the end of the dissertation mainly because of the following two reasons: (i) from a chronological point of view, this problem was studied after the previous two Chapters because the need for a deeper study of the human hand has been proved to be necessary, and (ii) to emphasize that the results here reported have not been used in the previous Chapters.

A universally accepted simplification of the human hand is to model each finger as a 4-DoFs serial manipulator. The first DoF exploits the abduction/adduction movement of the first phalanx with respect to the hand metacarpus (i.e. the motion in the frontal plane of the hand), whereas the other three DoFs exploit the flexion/extension movement of the three phalanges (i.e. a motion in the sagittal plane of the hand) of each finger. As universally accepted, a simplification of the complex motion of the hand is to consider the three flexion/extension revolute axis as parallel lines (Buchholz and Armstrong 1992; Bullock et al., 2012). Because of this last assumption, and disregarding

the abduction/adduction of the first phalange, the motion of the finger can be modelled as a planar motion. Of course, these simplifications lead to a simple but not very realistic model of the motion of the three phalanges. An improvement toward a more realistic model of the human hand is to consider the motion of the finger as a spatial motion where each phalanx rotates around lines that are not parallel to each other, i.e. are represented by skew lines in space. Given this interest, in this Chapter the problem to calculate the axis of rotation that model as best the motion of each finger phalange is tackled.

The axis identification procedures are used in several applications, such as the design and setting of prostheses, orthoses and exoskeletons, and the multibody modelling of human joints, e.g. lower limb and/or hand. Usually, the axis identification procedures need of the knowledge of the relative motion between of two bodies. Recently a new technique for the identification of these axes based on the theory of Burmester has been proposed in Sancisi et al. (2009). In this Chapter a refinement of this last technique is presented.

In Section 4.2, two novel procedures to identify the axis of rotation of the phalanges are presented. In Section 4.3, the description of the experimental measures devoted to acquire the spatial motion of each finger bone is reported, whereas Section 4.4 is devoted to the elaboration of the acquired experimental data. Finally, Section 4.5 shows and discusses the results of the proposed axis identification procedures also compared with a more standard technique based on the computation of the finite helical axis.

4.2 The proposed axis identification techniques

4.2.1 The Burmester theory

The Burmester theory is generally used for the synthesis of mechanisms (Burmester, 1877; Innocenti, 1995; Liao and McCarthy, 2001), but it is used here in an original way to identify an axis of rotation. The Burmester's theory states that given seven relative poses of two rigid bodies, up to 20 pairs of points (one on the first body and the other one on the second body) preserves their distance at all the seven poses. These points are called Burmester's points, BPs hereinafter. Particular degenerate solution of the Burmester problem can be achieved for special relative motions between the two rigid bodies. In

particular, a degenerate case is observed when the moving body (M) rotates about a fixed axis of the fixed body (F). In this case, all points of M do not change their distance from the points of F that lie on the rotation axis. From the mathematical point of view, the system of equations that describes the Burmester problem becomes singular, and the problem admits infinite solutions: the solution space for BPs on M coincides with the Cartesian space $\mathbb{R}^3$, whereas for the BPs on F it coincides with the line that represent the rotation axis. If the motion of M is only near to a rotation about a single fixed axis, the mathematical problem is definite and admits up to 20 solutions, as in the standard problem, but the BPs on F are nearly aligned in the neighbourhood of the rotation axis. The foregoing assumption is at the base of the axis identification procedure proposed in Sancisi et al. (2009). This procedure revealed a higher robustness to experimental inaccuracies, when compared to standard techniques based on mean and finite helical axis identification. In this Chapter, a refinement of this technique is proposed. In particular, when the moving body rotates about a fixed axis of the fixed body, the solution is twofold: the first solution, is the one above described, whereas the second is the symmetric one, thus the solution space for BPs on F coincides with the Cartesian space $\mathbb{R}^3$ and, for the BPs on M it coincides with the line that represent the rotation axis.

In Figure 4.1 a graphical representation of this statement is shown, where B_i and G_i ($i \leq 20$) are the BPs belonging to F and M respectively, whereas *a* is the axis of rotation fixed to F. Other two possible solutions, a sub case of the latter two, are that the BPs ($B_i - G_i$) coincides and/or both lies on the rotation axis. As a consequence, in a general case, for each pair of points $B_i - G_i$ at least one point of the pair can lie on the rotation axis whereas the other one not necessary lie on it. Similarly to what explained above, if the motion of M is only near to a rotation about a single fixed axis just half of the BPs are nearly aligned in the neighbourhood of the rotation axis, i.e. for each pair $B_i - G_i$ just one point of the pair can lie near the rotation axis whereas the other one not necessary lie on it. Based on this assumption the Burmester theory can be used to identify a revolute-joint model.

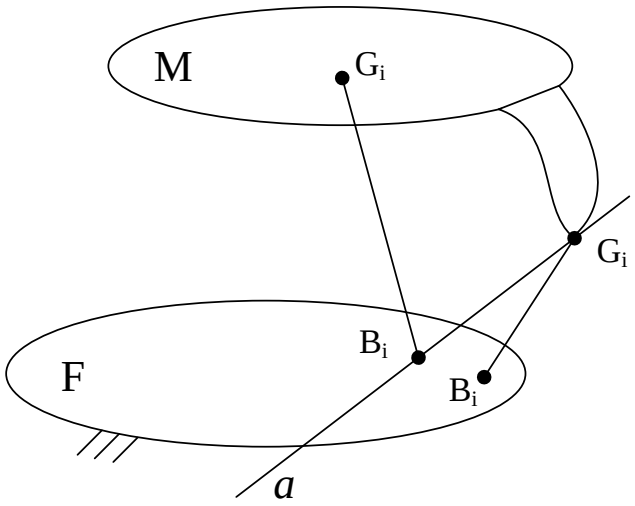

Figure 4.1 A graphical representation of the two possible solutions of the Burmester problem in the case that the moving body M rotates about a fixed axis (*a*) of the fixed body F. The points Bi (Gi) are the BPs belonging to F (M).

4.2.2 The revolute-joint model

A revolute-joint model essentially consists in two bodies constrained to rotate about a common axis of rotation, therefore the relative pose (position and orientation) of the two bodies is univocally identified by just one parameter i.e. the rotation θ about the common axis of rotation. Hereinafter the reference system associated to the first body is S_1 with coordinate axes x_1, y_1, z_1 and origin O_1 whereas the reference system associated to the second body is S_2 with coordinate axes x_2, y_2, z_2 and origin O_2. Generally speaking, an axis of rotation can be represented by a line in space, thus it is identified by its direction, represented by the unit vector **n** hereinafter, and by a point C on the line, represented by the position vector **c** hereinafter. A revolute-joint model can be viewed as two coincident lines, one in-built to S_1 and the other one in-built to S_2, yields collinear and with a prescribed relative translation λ along the line itself.

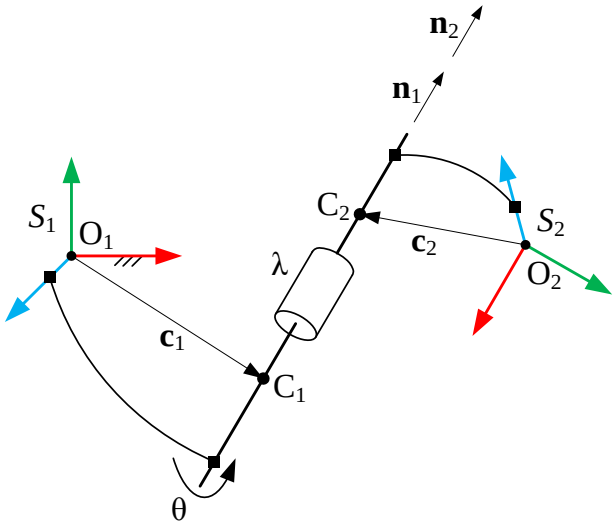

Figure 4.2 The revolute-joint model. The lines with squared ends stand for rigid connection between the two objects connected by the line itself.

With reference to Figure 4.2, $\mathbf{n}_1$ and $\mathbf{n}_2$ are the unit direction vectors of the two lines expressed in S_1 and S_2 respectively, $\mathbf{c}_1$ and $\mathbf{c}_2$ are the position vectors of the points C_1 and C_2 expressed in S_1 and S_2 respectively, whereas λ is the fixed distance between $\mathbf{C}_1$ and $\mathbf{C}_2$. Since $\mathbf{n}_1$ and $\mathbf{n}_2$ are vectors whose norm is unitary their components can be each expressed as a function of two independent parameters only, for instance the azimuth δ and the altitude η, y-z being the horizontal plane and z-axis the azimuth origin:

$$\mathbf{n}_1 = \begin{pmatrix} \sin\eta_1 \\ \cos\eta_1 \sin\delta_1 \\ \cos\eta_1 \cos\delta_1 \end{pmatrix} \quad \mathbf{n}_2 = \begin{pmatrix} \sin\eta_2 \\ \cos\eta_2 \sin\delta_2 \\ \cos\eta_2 \cos\delta_2 \end{pmatrix} \tag{4.1}$$

Furthermore, the position vectors $\mathbf{c}_1$ and $\mathbf{c}_2$ can be expressed in terms of the intersections of the same axis with the x-y reference plane, thus admitting the following representation:

$$\mathbf{c}_1 = \begin{pmatrix} C_{1x} \\ C_{1y} \\ 0 \end{pmatrix} \quad \mathbf{c}_2 = \begin{pmatrix} C_{2x} \\ C_{2y} \\ 0 \end{pmatrix} \tag{4.2}$$

It follows that nine geometrical independent parameters are needed to describe

a revolute-joint model. The pose of S_2 with respect to S_1 can be expressed by a 4x4 homogeneous moving matrix $\mathbf{T}^m$ obtained as the product of three 4x4 moving matrices:

$$\mathbf{T}^m = \mathbf{T}_{S1G1}\ \mathbf{T}_{G1G2}\ \left(\mathbf{T}_{S2G2}\right)^{-1} \tag{4.3}$$

The matrix $\mathbf{T}_{S1G1}$ ($\mathbf{T}_{S2G2}$) defines, with respect to S_1 (S_2), the pose of a reference system, here called S_{G1} (S_{G2}), having the z-axis collinear to the common line identified by $\mathbf{n}_1$ ($\mathbf{n}_2$) and the origin defined by the position vector $\mathbf{c}_1$ ($\mathbf{c}_2$). The matrix T_{G1G2} translates of λ and rotates of the angle θ about the z-axis thus defining the relative pose of S_{G2} with respect to S_{G1}. The matrix $\mathbf{T}^m$ can be written in the form $\mathbf{T}^m = \begin{pmatrix} \mathbf{R}^m & \mathbf{p}^m \\ 0 & 1 \end{pmatrix}$ where $\mathbf{R}^m$ is the 3x3 orthonormal matrix for the transformation of vector components from S_2 to S_1, whereas $\mathbf{p}^m$ is the position vector of the origin of S_2 expressed in S_1. The superscript *m* stands for "model".

4.2.3 The axis identification procedure

In this Section, the axis identification procedure is explained. It is important to highlight that the motion (i.e. a sequence of spatial poses) of each body is assumed to be known (e.g. from experimental measurements), so that it is possible to perform the axis identification procedure by analysing the relative poses between the two bodies. Hereinafter we refer to these poses as the "target poses" and the superscript *t* will be used.

Let S_1 (S_2) be the reference system associated to the fixed (moving) body F (M) and let $\mathbf{T}^t$ the 4x4 homogeneous matrices that define the pose of S_2 with respect to S_1. The matrix $\mathbf{T}^t$ can be written as $\mathbf{T}^t = \begin{pmatrix} \mathbf{R}^t & \mathbf{p}^t \\ 0 & 1 \end{pmatrix}$, where $\mathbf{R}^t$ is the 3x3 orthonormal matrix for the transformation of vector components from S_2 to S_1, whereas $\mathbf{p}^t$ is the position vector of the origin of S_2 expressed in S_1. The relative motion between the two bodies is given as a set of *n* matrices $\mathbf{T}_i^t$, that is *n* vectors $\mathbf{p}_i^t$ and matrices $\mathbf{R}_i^t$, where $i = 1,...,n$ and in general $n > 7$. The BPs are computed by taking a set *L* of seven poses randomly chosen from the whole set of the *n* poses. In this perspective, the spatial Burmester problem is given

by:

$$\left(\mathbf{b}_i^{(1)} - \mathbf{R}_j^t \mathbf{g}_i^{(2)} - \mathbf{p}_j^t\right)^2 = d_i^2, \ \forall j \in L \ , i \leq 20 \tag{4.4}$$

Where $\mathbf{b}_i^{(1)}$ is the position vector of the i-th point $\mathrm{B}_i^{(1)}$ belonging to F and represented in S_1, $\mathbf{g}_i^{(2)}$ is the position vector of the i-th point $\mathrm{G}_i^{(2)}$ belonging to M and represented in S_2, whereas d_i is the distance between $\mathrm{B}_i^{(1)}$ and $\mathrm{G}_i^{(1)}$ (where $\mathrm{G}_i^{(1)}$ is the point $\mathrm{G}_i^{(2)}$ represented in the system S_1, see Innocenti, 1995 for more details) at the given pose. Thus $\mathrm{B}_i^{(1)}$ and $\mathrm{G}_i^{(1)}$ (or equivalently $\mathrm{G}_i^{(2)}$) are the BPs. The solution of the Equation (4.4) can be computed both via numerical and via geometrical methods (Innocenti, 1995; Liao and McCarthy, 2001). In this Chapter the technique presented by Innocenti was implemented by using Maple®. To apply the axis identification procedure, N random combination L_k (where $k = 1,...,N$) must be defined and thus a number m of BPs, where in general $m \leq (20 \cdot N)$, can be obtained.

Among all the m BPs, one may need to discard the so called "outlier points". The outlier points are those pairs of points $\mathrm{B}_i^{(1)} - \mathrm{G}_i^{(1)}$ whose distance from a first-attempt-axis exceed a prescribed threshold $\bar{t}$. The first-attempt-axis may be found by approximating with a best-fitting line all the m BPs. For this purpose, the Theil-San linear regression technique (Siegel, 1982) was implemented because of its intrinsic robustness and independence by the presence of a great number (up to 50%) of outliers. The threshold $\bar{t}$ must be set according to the experience of the designers. To foster understanding of the text, the number of BPs who remains after the outlier elimination procedure are always denoted as m.

As stated above, just half of the m remaining BPs can lie on the searched axis, thus only $m' = m/2$ of the m BPs can be useful for the axis identification technicque, i.e. are more aligned in the neighbourhood of the searched optimal-axis, whereas the other $m/2$ BPs can be consequently discarded. In order to find the m' more-aligned BPs, the following technique was used.

First, take the points $\mathrm{G}_i^{(1)}$ expressed in S_1, then choose a set of m' BPs, taking

just one point for each pair of points $B_i^{(1)} - G_i^{(1)}$, and then approximate the set of the m' points by a best-fitting line, then compute the actual distance of each point by the new line and finally compute the value of the function f_d defined as the sum of the squared actual distances of each point $B_i^{(1)} - G_i^{(1)}$ by the new line. The set of m' points that minimize the function f_d is the set of points that are more aligned along the searched optimal-axis. Theoretically, in order to find the optimal set of the m' points among the *m* BPs that minimize the function f_d, all the possible combinations have to be computed. Practically, given *m* pairs of BPs, all the possible combinations *K* of the m' points taken in pairs of two among all the *m* BPs, are $K = 2^{m'}$, thus e.g. if $m = 100$ then $K = 2^{50} \approx 10^{15}$ consequently resulting computationally infeasible and/or inefficient to compute all the possible *K* combinations. Therefore, this procedure was implemented as a numerical optimization by means of the Matlab® Genetic Algorithm Toolbox. In particular, the numerical optimization procedure aims to find the vector $\mathbf{x} \in \mathbb{R}^{m'}$ whose elements are defined as:

$$\mathbf{x}_i = \begin{cases} 0 & \text{if } B_i^{(1)} \text{ is chosen} \\ 1 & \text{if } G_i^{(1)} \text{ is chosen} \end{cases} \quad \text{where } i = 1,\ldots,m' \tag{4.5}$$

Thus the optimization problem is defined as:

$$\min_{\mathbf{x}} f_d \tag{4.6}$$

where the function f_d is above defined. Once the vector **x** is found, the BPs that are more aligned along the searched optimal-axis were identified. The optimal-axis identification procedure can now be split into two different techniques. The first technique aims to find only the fixed axis in-built to S_1, called a_1 hereinafter , whereas the second technique aims to find in addition the moving axis in-built to S_2, called a_2 hereinafter, and the parameter λ, thus completely defining the revolute-joint model.

4.2.3.1 The first technique

Once the vector **x** is found, let take the associated point cloud composed by all the pairs of points $B_i^{(1)} - G_i^{(1)}$ and approximate it by a best-fitting line by means

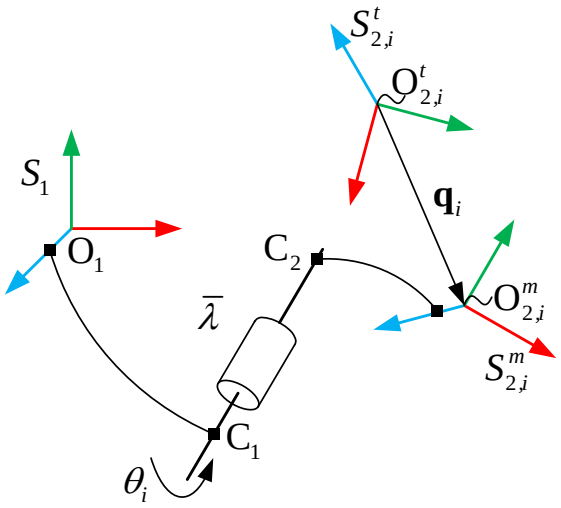

Figure 4.3 $S^*_{2,i}$ is the moving-body system of the revolute-joint model, whereas $S_{2,i}$ is the moving-body system of the target motion.

of a linear regression technique (e.g. by a standard least-square technique). Since the points $B^{(1)}_i - G^{(1)}_i$ are expressed in S_1, the resulting axis a_1 is a fixed axis in-built to S_1.

4.2.3.2 The second technique

Once the vector **x** is found, let define the associated point cloud composed by the points $B^{(1)}_i$ ($G^{(2)}_i$) and approximate it by a best-fitting line in order to find the axis a_1 (a_2) in-built to S_1 (S_2). In order to univocally define the revolute-joint model that best-fit all the target poses, a two-step procedure is here explained.

The first step

The first step of the procedure aims to finds the n angles θ_i which leads $S^m_{2,i}$ closest to $S^t_{2,i}$ (where $i = 1,..,N$) in terms only of rotation parameters. In Figure 4.3 a picture representing the i-th pose of the systems $S^t_{2,i}$ and $S^m_{2,i}$ is reported.

Let parameterize each rotation matrix $\mathbf{R}^m_i$ (that is $\mathbf{R}^t_i$) by using three angles $\alpha^m_i, \beta^m_i, \gamma^m_i$ (that is $\alpha^t_i, \beta^t_i, \gamma^t_i$), thus $\mathbf{R}^m_i = \mathbf{R}^m_i\left(\alpha^m_i, \beta^m_i, \gamma^m_i\right)$ and $\mathbf{R}^t_i = \mathbf{R}^t_i\left(\alpha^t_i, \beta^t_i, \gamma^t_i\right)$. Any parameterization for the orientation can be chosen.

The values of the *n* angles θ_i which leads $S_{2,i}^m$ closest to $S_{2,i}^t$ in terms of rotation parameters (i.e., $\alpha_i^m, \beta_i^m, \gamma_i^m$ and $\alpha_i^t, \beta_i^t, \gamma_i^t$), can be obtained by finding the angle θ_i that guarantee that $\alpha_i^m = \alpha_i^t$ (or equivalently $\beta_i^m = \beta_i^t$ or $\gamma_i^m = \gamma_i^t$). The author's suggestion is to choose the orientation parameter α (that is β or γ) as the one that, among the three orientation parameters, has the grater angular excursion during the whole given motion. Once the *n* angles θ_i were found, the orientation of the system $S_{2,i}^m$, i.e. the matrices $\mathbf{R}_i^m$, is univocally determined.

The second step

The second step of the procedure aim to find the particular value $\bar{\lambda}$ of the parameter λ that guarantees a best fitting of all the systems $S_{2,i}^m$ to $S_{2,i}^t$ for $i = 1,..,N$ in terms of position. It is worth noting that a translation along the common axis of rotation (i.e. the axis obtained putting collinear the two axes a_1 and a_2) does not effects the orientation of the system $S_{2,i}^m$, but only its position with respect to S_1.

Let $\mathbf{q}_i$ be the position vector of the origin $\mathrm{O}_{2,i}^m$ with respect to $\mathrm{O}_{2,i}^t$ expressed in S_1, thus defined by the following equation:

$$\mathbf{q}_i = \left(\mathbf{o}_{2,i}^m - \mathbf{o}_{2,i}^t\right) = \left(\mathbf{c}_1 + \lambda \mathbf{n}_1 - \mathbf{R}_i^m \mathbf{c}_2\right) - \mathbf{o}_{2,i}^t \tag{4.7}$$

Where $\mathbf{o}_{2,i}^m$ ($\mathbf{o}_{2,i}^t$) is the position vector of the origin $\mathrm{O}_{2,i}^m$ ($\mathrm{O}_{2,i}^t$) expressed in S_1.

Let $|\mathbf{q}_i|^2$ be the square norm of the vector $\mathbf{q}_i$. Putting the derivative of $\frac{\partial |\mathbf{q}_i|^2}{\partial \lambda}$ to zero will yield the following values of λ_i:

$$\lambda_i = \left(-\mathbf{c}_1 + \mathbf{R}_i^m \mathbf{c}_2 + \mathbf{p}_i^t\right) \cdot \mathbf{n}_1 = \mathbf{v}_i \cdot \mathbf{n}_1 \quad \text{where} \quad i = 1,..,N \tag{4.8}$$

The *n* values λ_i identify the translational parameters along the axis needed to minimize each length $|\mathbf{q}_i|^2$ between the origins of the systems $S_{2,i}^m$ and $S_{2,i}^t$. Since a unique value for λ is necessary to univocally define the revolute-joint model, the following objective function (*FO*) can be minimized:

$$FO = \frac{1}{N}\sum_{i=1}^{N}\left|\mathbf{q}_i\right|^2 \tag{4.9}$$

The function *FO* expresses the mean value of the square norm of each vector $\mathbf{q}_i$. The minimum of the Equation (4.9) with respect to λ can be computed as:

$$\begin{aligned}
&min\ FO = \frac{1}{N}\sum_{i=1}^{N}\left|\mathbf{q}_i\right|^2 \Rightarrow \frac{\partial}{\partial\lambda}\left(\frac{1}{N}\sum_{i=1}^{N}\left|\mathbf{q}_i\right|^2\right) = 0 \Rightarrow \\
&\frac{\partial}{\partial\lambda}\left(\frac{1}{N}\sum_{i=1}^{N}\left|\mathbf{q}_i\right|^2\right) = \frac{1}{N}\left(\sum_{i=1}^{N}\frac{\partial\left|\mathbf{q}_i\right|^2}{\partial\lambda}\right) = \frac{1}{N}\left(\sum_{i=1}^{N}\bar{\lambda} - \mathbf{v}_i\cdot\mathbf{n}_1\right) = \\
&= \bar{\lambda} - \frac{1}{N}\sum_{i=1}^{N}\mathbf{v}_i\cdot\mathbf{n}_1 = \bar{\lambda} - \frac{1}{N}\sum_{i=1}^{N}\lambda_i = 0 \Rightarrow \\
&\Rightarrow \bar{\lambda} = \frac{1}{N}\sum_{i=1}^{N}\lambda_i
\end{aligned} \tag{4.10}$$

Thus, the searched optimal value $\bar{\lambda}$ of the parameter λ is the mean value of the *N* values λ_i (where $i = 1,..,N$) that minimize each length $\left|\mathbf{q}_i\right|^2$ between the origins of the systems $S_{2,i}^m$ and $S_{2,i}^t$.

In conclusion, all the parameters needed to define the revolute-joint model, i.e. the parameters needed to define the two axes a_1 and a_2 and the parameter $\bar{\lambda}$, are now determined.

4.3 Experimental measures

The aim of the experimental tests is to measure simultaneously the spatial motion of both one finger and the palm of the hand of a healthy subject. The three phalanges of the finger and the palm are here considered as rigid bodies. This last assumption is reasonable and universally accepted for finger bones (Buchholz et al., 1992; Bullock et al., 2012), whereas for the palm is usually accepted even if less reasonable with respect to the previous one.

The motion of each bone is acquired by the use of the Vicon® system, a well-known stereo-photogrammetric device able to acquire the spatial motion of

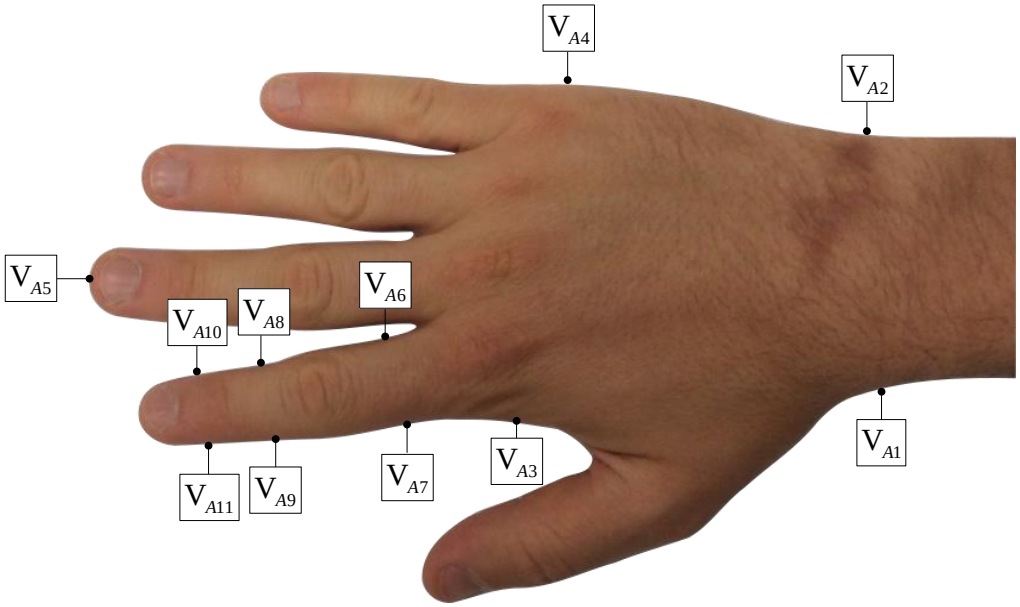

Figure 4.4 The repere points to be identified.

passive markers, i.e. plastic sphere covered by a retro-reflective paint.

Generally speaking, in order to define the spatial pose of a rigid body is sufficient to know the spatial position of three points belonging to the body itself. In this perspective, by using the Vicon® system, it is sufficient to attach three passive markers to each bone in order to obtain informations on its spatial pose. Usually, the three markers are attached to a rigid support, called the tracker hereinafter, which is fixed to the moving bone. In particular, the Vicon® system can measure the spatial position of the centre of each marker at a given rate f (measured in Hz), thus the continuous motion of the markers (that is of the body) is discretized in a total number of frames N given by $N = f \cdot T$, where T is the duration time (measured in seconds) of the experimental acquisition.

In the following, the procedure used to measure the spatial motion of the hand is reported.

4.3.1 Definition of the repere points

Firstly, some "repere points" must be identified. The repere points are particular points of the human hand anatomy - that can be identified by direct palpation of the human finger - and that do not change their position during the motion of the finger itself. In Figure 4.4, the eleven repere points that must be identified

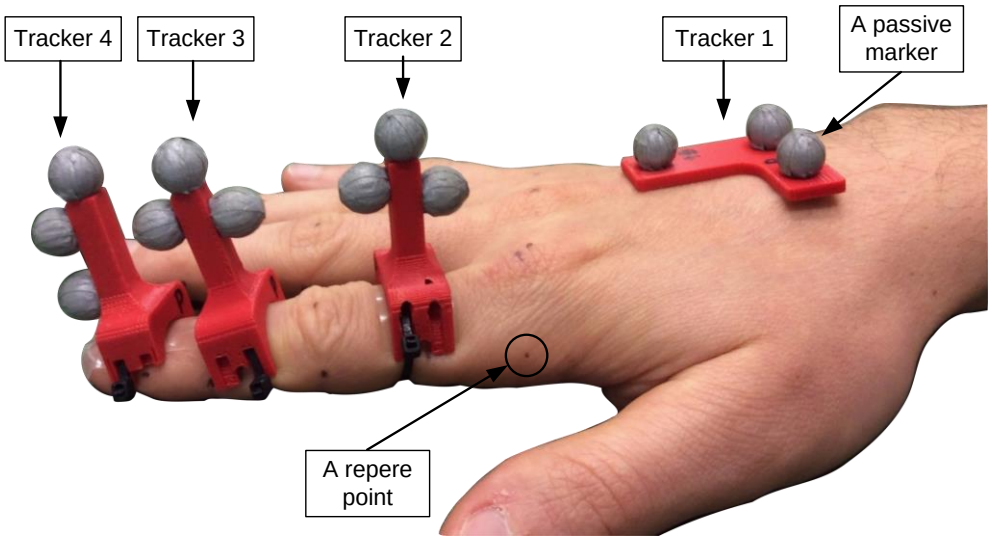

Figure 4.5 The experimental setup.

are reported. The point V_{A1} (V_{A2}) is located at the radial (ulnar) styloid process. The point V_{A3} (V_{A4}) is located in the radio-ulnar plane at the point of greatest protrusion of the MCP joint of the second (fifth) finger.

Moreover, the point V_{A5} is located in the radio-ulnar plane at the fingertip of the middle finger. The points V_{A6} and V_{A7} (V_{A8} and V_{A9}) are located in the radio-ulnar plane at half of the thickness of the first (second) phalange - measured in the sagittal plane - at the position where the thickness of the finger - measured in the coronal plane - is minimal. Similarly, the points V_{A10} and V_{A11} are located in the radio-ulnar plane at half of the thickness of the third phalange - measured in the sagittal plane - immediately after perceived the prominence of the DIP joint.

4.3.2 The trackers

To each phalange and to the dorsal side of the hand, trackers supporting three passive markers of diameter $d = 9.5$ mm each, are attached. In Figure 4.5, a picture showing the four trackers is reported. The Tracker 1, must be put approximately on the center of the dorsal side of the hand, and stick to the hand by using double-sided tape. The trackers 2-4 have a suitably shaped side ad hoc designed to be putted approximately in the middle of each finger phalange (further details in the following). In particular, the trackers have lateral holes

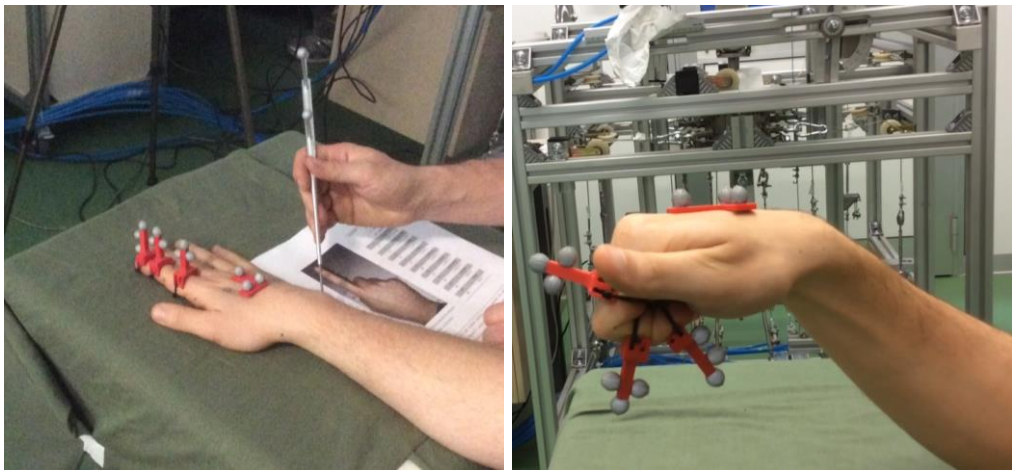

a) b)

Figure 4.6 a) Acquisition of the repere points by using the pointer. b) Acquisition of the full flexion motion of the finger.

useful to choose the right relative position of the tracker with respect to the phalange. The trackers must be put on the phalange in such a way that the repere points V_{A6-11} lie approximately centred into the lateral holes. These last three trackers are stick to the finger phalange by double-side tape and are also fastened by plastic strips.

4.3.3 Experimental measures by the Vicon® system

The experimental measures are divided into two steps. The first step aims to acquire the repere points previously defined, whereas the second step aims to acquire the motion of the finger.

The repere points are acquired by using the pointer shown in Figure 4.6a. The pointer is a rigid body with a long shape and a small spherical tip. Three markers are fixed to the pointer and the geometry of the pointer, i.e. the relative distance of the pointer tip and the three markers, is completely known. Thus, by acquiring the spatial position of the three markers, informations on the spatial position of the pointer tip can be obtained.

The subject must rest the palm and the forearm in a prone position on a table, the middle finger must be aligned with the forearm. With reference to this static position of the hand, all the repere points must be acquired by touching with the pointer tip each repere point.

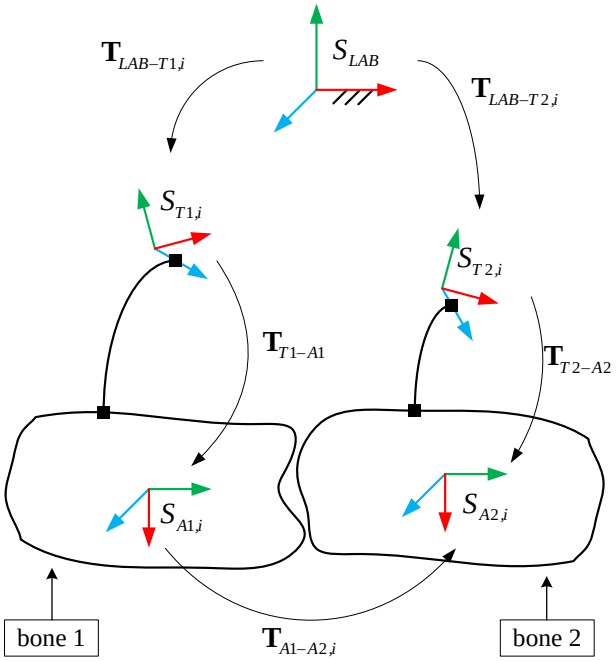

Figure 4.7 The reference system and the transformation matrices needed to get the relative motion between the two bones. The trackers are not shown. The lines with squared ends represent a rigid connection between two elements.

Finally, the full flexion-extension motion of the finger (see Figure 4.6b) was acquired five times per each finger. The motion of the index, the middle and the ring finger of a healthy subjects was acquired.

4.4 Elaboration of the experimental data

The aim of this Section is to obtain the relative motion between two adjacent bones. In this Section, in order to explain the procedure by means of an example, the relative motion between the bone 1 (the wrist) and the bone 2 (the first phalange) is obtained. The relative motion between different bones can be easily obtained by generalizing the following procedure.

With reference to Figure 4.6, S_{LAB} is the Vicon® reference system, $S_{A1,i}$ and $S_{A2,i}$ are the anatomical systems associated to the two bones, whereas $S_{T1,i}$ and $S_{T2,i}$ are the technical systems associated to the trackers fixed to the same bones. Moreover, $\mathbf{T}_{LAB-T1,i}$ ($\mathbf{T}_{LAB-T2,i}$) is the 4x4 homogeneous matrix that

defines the actual pose of the system $S_{T1,i}$ ($S_{T2,i}$) with respect to S_{LAB}, whereas $\mathbf{T}_{T1-A1}$($\mathbf{T}_{T2-A2}$) defines the pose of the system $S_{A1,i}$ ($S_{A2,i}$) with respect to $S_{T1,i}$ ($S_{T2,i}$). Finally, $\mathbf{T}_{A1-A2,i}$ defines the actual pose of the system $S_{A2,i}$ with respect to $S_{A1,i}$. The matrix $\mathbf{T}_{A1-A2,i}$ can be obtained as:

$$\mathbf{T}_{A1-A2,i} = \left(\mathbf{T}_{LAB-T1,i}\,\mathbf{T}_{T1-A1}\right)^{-1}\left(\mathbf{T}_{LAB-T2,i}\,\mathbf{T}_{T2-A2}\right) \tag{4.11}$$

Where $(\bullet)^{-1}$ stand for the inverse of the matrix inside brackets. The subscript *i* refers to the *i*-th frame acquired by the Vicon® system, thus $i = 1,..,N$ where N is the total number of frames acquired during the experimental test. It is worth noting that since the relative position from the trackers and the bones is supposed to be fixed during the finger motion, for the matrices $\mathbf{T}_{T1-A1}$ and $\mathbf{T}_{T2-A2}$ the subscript *i* does not appear.

4.4.1 Definition of the technical systems

The matrix $\mathbf{T}_{LAB-T1,i}$ can be written in the form $\mathbf{T}_{LAB-T1,i} = \begin{pmatrix} \mathbf{R}_{LAB-T1,i} & \mathbf{p}^{(LAB)}_{LAB-T1,i} \\ \mathbf{0} & 1 \end{pmatrix}$

where $\mathbf{R}_{LAB-T1,i}$ is the 3x3 orthonormal rotation matrix for the transformation of the vector components from $S_{T1,i}$ to S_{LAB}, $\mathbf{p}^{(LAB)}_{LAB-T1,i}$ is the position vector of the origin of $S_{T1,i}$ written in S_{LAB}, whereas **0** is the 1x3 null vector. Let the points $M_{j,i}$ (where $j = 1,2,3$ and $i = 1,..,N$) be the centres of the three markers attached to a generic tracker and let $\mathbf{m}^{(LAB)}_{j,i}$ the position vectors of these points written in S_{LAB}. It is worth noting that the components of the position vectors $\mathbf{m}^{(LAB)}_{j,i}$ are the output of the Vicon® system. To be lighter on the mathematical notation, an additional subscript that references the tracker was not added. Given the three vectors $\mathbf{m}^{(LAB)}_{j,i}$ the vector $\mathbf{p}^{(LAB)}_{LAB-T1,i}$ and the matrix $\mathbf{R}_{LAB-T1,i}$, i.e. the pose of the system $S_{T1,i}$ with respect to S_{LAB}, can be defined as follows. $\mathbf{p}^{(LAB)}_{LAB-T1,i}$ can be defined as the position vector of the centroid of the points $M_{j,i}$, thus :

$$\mathbf{p}_{LAB-T1,i}^{(LAB)} = \frac{1}{3}\sum_{j=1}^{3}\mathbf{m}_{j,i}^{(LAB)} \tag{4.12}$$

As regards the matrix $\mathbf{R}_{LAB-T1,i}$ it is worth noting that the columns of the rotation matrix are the unit vectors of the three coordinate axes of the system $S_{T1,i}$ written in S_{LAB}, thus:

$$\begin{aligned}
\mathbf{x}_{T1,i}^{(LAB)} &= \frac{\left(\mathbf{m}_{1,i}^{(LAB)} - \mathbf{m}_{2,i}^{(LAB)}\right)}{\left|\mathbf{m}_{1,i}^{(LAB)} - \mathbf{m}_{2,i}^{(LAB)}\right|} \\
\mathbf{y}_{T1,i}^{(LAB)} &= \frac{\left(\mathbf{m}_{1,i}^{(LAB)} - \mathbf{m}_{2,i}^{(LAB)}\right)\times\left(\mathbf{m}_{1,i}^{(LAB)} - \mathbf{m}_{3,i}^{(LAB)}\right)}{\left|\mathbf{m}_{1,i}^{(LAB)} - \mathbf{m}_{2,i}^{(LAB)}\right|\left|\mathbf{m}_{1,i}^{(LAB)} - \mathbf{m}_{3,i}^{(LAB)}\right|} \\
\mathbf{z}_{T1,i}^{(LAB)} &= \mathbf{x}_{T1,i}^{(LAB)} \times \mathbf{y}_{T1,i}^{(LAB)} \\
\Rightarrow \quad \mathbf{R}_{LAB-T1,i} &= \left(\mathbf{x}_{T1,i}^{(LAB)} \quad \mathbf{y}_{T1,i}^{(LAB)} \quad \mathbf{z}_{T1,i}^{(LAB)}\right)
\end{aligned} \tag{4.13}$$

Where $\mathbf{x}_{T1,i}^{(LAB)}$, $\mathbf{y}_{T1,i}^{(LAB)}$ and $\mathbf{z}_{T1,i}^{(LAB)}$ must be column vectors, whereas $|\bullet|$ stand for the norm of the vector inside brackets. The procedure here explained can be used also for the definition of the actual pose of the other technical systems $S_{Tj,i}$ where $j = 2,..,4$.

4.4.2 Definition of the anatomical system of the wrist

Similarly to matrix $\mathbf{T}_{LAB-T1,i}$, the matrix $\mathbf{T}_{T1-A1}$ can also be written in the form $\mathbf{T}_{T1-A1} = \begin{pmatrix} \mathbf{R}_{T1-A1} & \mathbf{p}_{T1-A1}^{(T1)} \\ \mathbf{0} & 1 \end{pmatrix}$. The pose of the system $S_{A1,i}$ with respect to $S_{T1,i}$, can be obtained as follows. Firstly, once the $\mathbf{T}_{LAB-T1,i}$ is determined, the repere points $\mathrm{V}_{A1} - \mathrm{V}_{A5}$ coordinates can be transformed from S_{LAB} to the technical system $S_{T1,i}$, so that the vectors $\mathbf{v}_{A1}^{(T1)} - \mathbf{v}_{A5}^{(T1)}$ can be obtained. Then $\mathbf{p}_{T1-A1}^{(T1)}$ can be defined as the position vector of the centroid of the points V_{A1} and V_{A2}, thus:

$$\mathbf{p}_{T1-A1}^{(T1)} = \frac{\mathbf{v}_{A1}^{(T1)} + \mathbf{v}_{A2}^{(T1)}}{2} \tag{4.14}$$

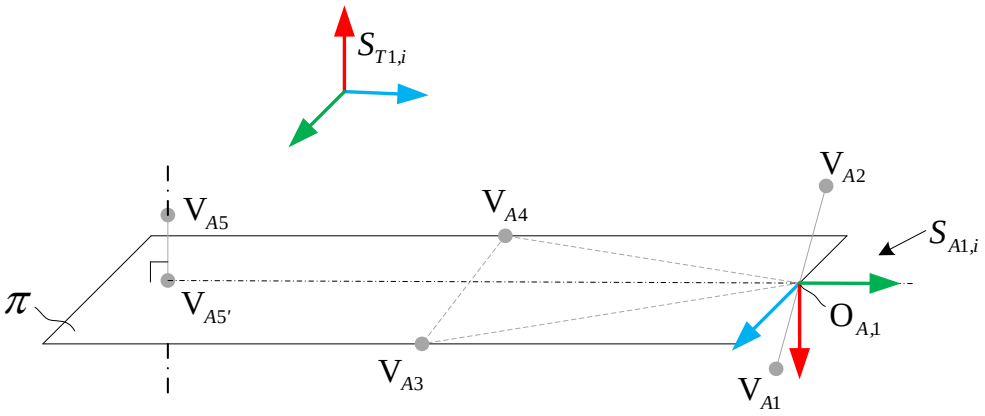

Figure 4.8 The anatomical system of the wrist.

With reference to Figure 4.8, the plane π is the plane containing the points identified by the position vectors $\mathbf{p}_{T1-A1}^{(T1)}$, $\mathbf{v}_{A3}^{(T1)}$ and $\mathbf{v}_{A4}^{(T1)}$. The point $V_{A5'}$ is the projection of the point V_{A5} on the plane π and the vector $\mathbf{v}_{A5'}^{(T1)}$ expresses its position. Once again, the column of the matrix $\mathbf{R}_{T1-A1}$ are the unit vectors of the three coordinate axes of the system $S_{A1,i}$ written in $S_{T1,i}$, thus:

$$\begin{aligned}
\mathbf{x}_{A1}^{(T1)} &= \frac{\left(\mathbf{v}_{A3}^{(T1)} - \mathbf{p}_{T1-A1}^{(T1)}\right) \times \left(\mathbf{v}_{A4}^{(T1)} - \mathbf{p}_{T1-A1}^{(T1)}\right)}{\left|\mathbf{v}_{A3}^{(T1)} - \mathbf{p}_{T1-A1}^{(T1)}\right| \left|\mathbf{v}_{A4}^{(T1)} - \mathbf{p}_{T1-A1}^{(T1)}\right|} \\
\mathbf{y}_{A1}^{(T1)} &= \frac{\left(\mathbf{p}_{T1-A1}^{(T1)} - \mathbf{v}_{A5'}^{(T1)}\right)}{\left|\mathbf{p}_{T1-A1}^{(T1)} - \mathbf{v}_{A5'}^{(T1)}\right|} \\
\mathbf{z}_{A1}^{(T1)} &= \mathbf{x}_{A1}^{(T1)} \times \mathbf{y}_{A1}^{(T1)} \\
\\
\Rightarrow \quad \mathbf{R}_{T1-A1} &= \left(\mathbf{x}_{A1}^{(T1)} \quad \mathbf{y}_{A1}^{(T1)} \quad \mathbf{z}_{A1}^{(T1)}\right)
\end{aligned} \tag{4.15}$$

Once again, the vectors $\mathbf{x}_{A1,i}^{(T1)}$, $\mathbf{y}_{A1,i}^{(T1)}$ and $\mathbf{z}_{A1,i}^{(T1)}$ are column vectors.

4.4.3 Definition of the anatomical system of the phalange

The matrix $\mathbf{T}_{T2-A2}$ can be written in the form $\mathbf{T}_{T2-A2} = \begin{pmatrix} \mathbf{R}_{T2-A2} & \mathbf{p}_{T2-A2}^{(T2)} \\ \mathbf{0} & 1 \end{pmatrix}$. The pose of the system $S_{A2,i}$ with respect to $S_{T2,i}$, can be obtain as follows. Once

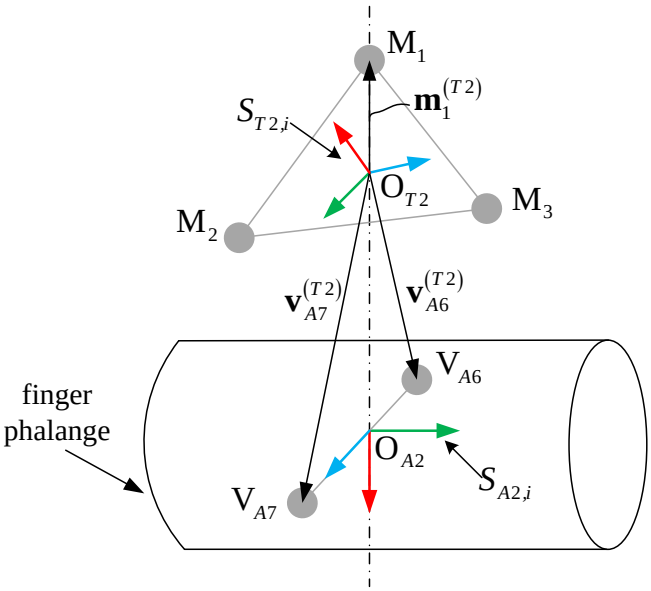

Figure 4.9 The anatomical system of the first phalange.

the matrix $\mathbf{T}_{LAB-T2,i}$ is determined, the coordinates of the repere points V_{A6} and V_{A7} from S_{LAB} can be transformed to the technical system $S_{T2,i}$, and the vectors $\mathbf{v}_{A6}^{(T2)}$ and $\mathbf{v}_{A7}^{(T2)}$ can be obtained. With reference to Figure 4.9, let number the markers of the tracker fixed to the phalange in such a way that the marker M_1 is the one placed on the top of the tracker (i.e. the one placed in the most distal position from the finger phalange) and determine the position vector $\mathbf{m}_1^{(T2)}$. $\mathbf{p}_{T2-A2}^{(T2)}$ is the position vector of the centroid of the points V_{A6} and V_{A7}, i.e.:

$$\mathbf{p}_{T2-A2}^{(T2)} = \frac{\mathbf{v}_{A6}^{(T2)} + \mathbf{v}_{A7}^{(T2)}}{2} \tag{4.16}$$

Once again, the column of the matrix $\mathbf{R}_{T2-A2}$ are the unit vectors of the three coordinate axes of the system $S_{A2,i}$ written in $S_{T2,i}$, thus:

$$\begin{aligned}
\mathbf{x}_{A2}^{(T2)} &= \frac{\left(\mathbf{p}_{T2-A2}^{(T2)} - \mathbf{m}_{1}^{(T2)}\right)}{\left|\mathbf{p}_{T2-A2}^{(T2)} - \mathbf{m}_{1}^{(T2)}\right|} \\
\mathbf{y}_{A2}^{(T2)} &= \frac{\left(\mathbf{m}_{1}^{(T2)} - \mathbf{v}_{A7}^{(T2)}\right) \times \left(\mathbf{m}_{1}^{(T2)} - \mathbf{v}_{A6}^{(T2)}\right)}{\left|\mathbf{m}_{1}^{(T2)} - \mathbf{v}_{A7}^{(T2)}\right| \left|\mathbf{m}_{1}^{(T2)} - \mathbf{v}_{A6}^{(T2)}\right|} \\
\mathbf{z}_{A2}^{(T2)} &= \mathbf{x}_{A2}^{(T2)} \times \mathbf{y}_{A2}^{(T2)} \\
\\
\Rightarrow \quad \mathbf{R}_{T2-A2} &= \left(\mathbf{x}_{A2}^{(T2)} \quad \mathbf{y}_{A2}^{(T2)} \quad \mathbf{z}_{A2}^{(T2)}\right)
\end{aligned} \tag{4.17}$$

Where, again, $\mathbf{x}_{A2}^{(T2)}$, $\mathbf{y}_{A2}^{(T2)}$ and $\mathbf{z}_{A2}^{(T2)}$ must be column vectors. The anatomical systems of the second and third phalange can be obtained similarly to the one obtained here for the first phalange.

It is worth to highlight that the anatomical systems thus defined, are in good (but not full) agreement with the ISB standard recommendations (Wu et al., 2005). Indeed, the anatomical systems proposed by the ISB standard recommendations need of the full knowledge of the human bones. However, the methodology here presented to define the anatomical systems permits to identify such systems quite accurately in terms of final pose, if compared to the one suggested by the ISB.

4.4.4 The relative pose between two adjacent bones

The matrix $\mathbf{T}_{A1-A2,i} = \begin{pmatrix} \mathbf{R}_{A1-A2,i} & \mathbf{p}_{A1-A2,i}^{(A1)} \\ \mathbf{0} & 1 \end{pmatrix}$ expresses the actual relative pose between two anatomical systems $S_{A1,i}$ and $S_{A2,i}$. The rotational matrix $\mathbf{R}_{A1-A2,i}$ can be parameterized as a function of three angles α_i , β_i and γ_i as follows:

$$\mathbf{R}_{A1-A2,i} = \begin{pmatrix} c_{\alpha_i} c_{\gamma_i} + s_{\alpha_i} s_{\beta_i} s_{\gamma_i} & -s_{\alpha_i} c_{\gamma_i} + c_{\alpha_i} s_{\beta_i} s_{\gamma_i} & -c_{\beta_i} s_{\gamma_i} \\ s_{\alpha_i} c_{\beta_i} & c_{\alpha_i} c_{\beta_i} & s_{\beta_i} \\ c_{\alpha_i} s_{\gamma_i} - s_{\alpha_i} s_{\beta_i} c_{\gamma_i} & -s_{\alpha_i} s_{\gamma_i} - c_{\alpha_i} s_{\beta_i} c_{\gamma_i} & c_{\beta_i} c_{\gamma_i} \end{pmatrix} \tag{4.18}$$

where c and s are the cosine and sine of the angle in subscript and α_i , β_i and γ_i are the actual flexion/extension, ab/adduction and intra/extra rotation angles of the first bone relatively to the second one, using the Grood-and-Suntay joint

coordinate system convention (Grood and Suntay, 1983). The subscript *i*, as usual, refers to the actual i-th frame of the acquisition.
According to Grood-and-Suntay convention, the flexion/extension movement is a rotation about the z-axis of the system $S_{A1,i}$ (flexion is positive), the intra/extra movement is a rotation about the y-axis of the system $S_{A2,i}$ (external rotation is positive), whereas the ab/adduction movement is a rotation about a floating axis perpendicular to the previous ones (adduction is positive). Expression (4.18) can be applied for right hands, in order to use the Grood and Suntay convention for left hand the systems $S_{A1,i}$ and $S_{A2,i}$ have to be appropriately defined for left-hand bones according to Wu et al. (2005).

During the experimental tests, the spatial motion of three fingers (the index, the middle and the ring) of the right hand of a healthy subject of 37 years old was acquired. The hand of the subject was 200 mm in length and 90 mm in width.

As stated above, the full flexion motion of each finger was acquired for five times. For each acquisition, by using Equation (4.11), the relative motion between adjacent bones is obtained. As an example, in Figure 4.10, five graphs representing the pose parameters of the relative motion between the anatomical systems of the wrist and the first phalange of the index finger are reported. In particular, the three graphs on the left (from top to bottom) represent the three components of the position vector $\mathbf{p}_{A1-A2}^{(A1)}$, whereas the other two graphs represent the trend of the angle β (ab/adduction) and the angle γ (intra/extra). All graphs are represented as function of the flexion angle (α).

Each graph in Figure 4.10 reports six lines: five thin random coloured lines represent the five acquisitions, whereas the blue thick line represents the "average motion" and the standard deviation (vertical lines) of the five acquisitions. Similar graphs were obtained for the relative motion of adjacent bones of the three measured fingers.

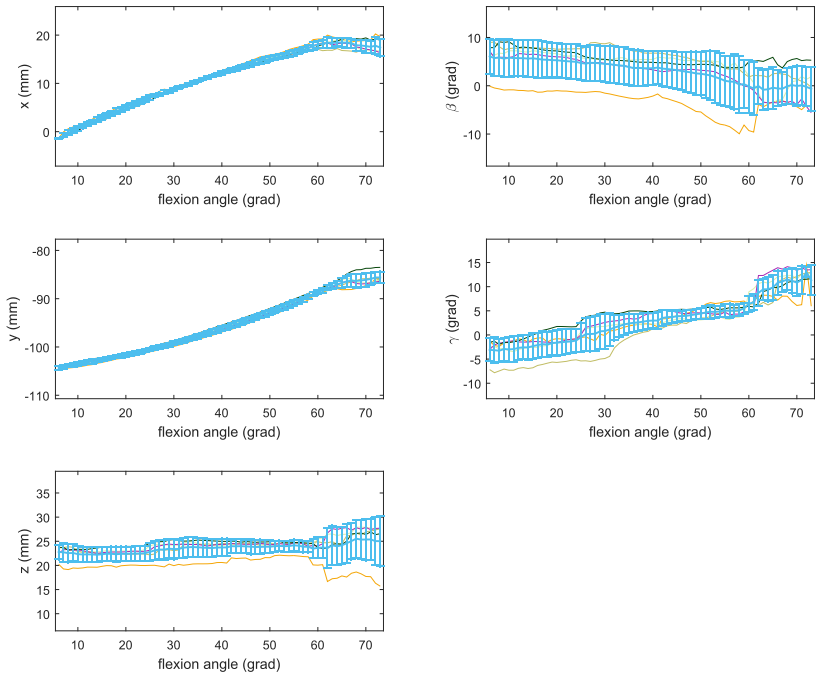

Figure 4.10 The motion parameters for the relative motion between the wrist and the first phalange of the index finger. The thin random colored lines represent the five acquisitions. The blue thick line represents the average motion (computed considering the five acquisition), whereas vertical blue thick liners represents the standard deviation of the five acquisition.

4.5 Joint axes identification: results and discussions

In this Section, the axes identification techniques of Section 4.2 in addition to the well-known helical axis identification technique are applied and discussed. The resulting average motion (Section 4.3) was taken as the "given motion" necessary to the application of the axes identification techniques.

For the helical axis (HA) technique, the revolute joint model is identified by calculating the screw axis from the pose at the 33% and the pose at the 66% of the range of motion of the flexion angle, and by associating the resulting axis to the first one of the two chosen poses. For the Burmester 1° (B1) technique, the revolute joint model is completely defined by associating the resulting axis to the pose corresponding to the 33% of the flexion angle range of motion,

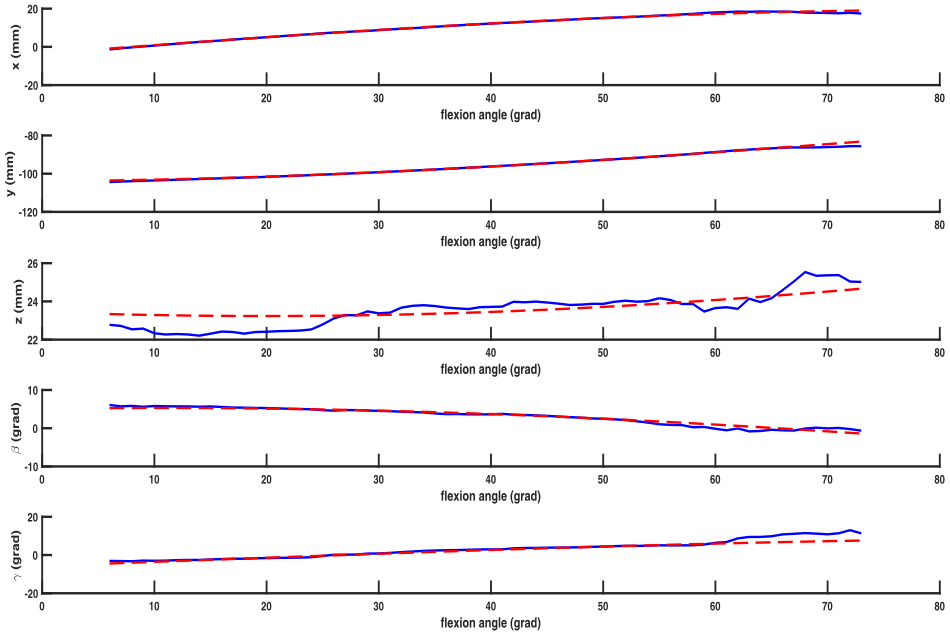

Figure 4.11 Pose parameters of the wrist and first phalange motion. Solid = experimental data; Dot = model. The model is identified by the HA technique.

whereas for the Burmester 2° (B2) technique, as explained in Section 4.2, the technique aim to find itself a complete revolute joint model.

In Figure 4.11-13 the trends of the pose parameters of the given motion and of the revolute-joint-model motion are reported. The three graphs only refers to the relative motion between the bone 1 (the wrist) and the bone 2 (the first phalange) of the index finger. In particular Figure 4.11 refers to the results obtained by using the HA technique, Figure 4.12 shows the results found by using the B1 technique, whereas Figure 4.13 shows the results found by using the B2 technique. Once again, similar graphs were obtained for the relative motion of adjacent bones of the three measured fingers.

In Table 4.1, the mean absolute errors computed for the three translational parameters and for the two rotational parameters between the experimental measure and the resulting model of the adjacent bones of the three fingers are reported.

The results, in terms of mean absolute error, are in general very good. In particular, the values of the translational errors e_x, e_y and e_z are very good for

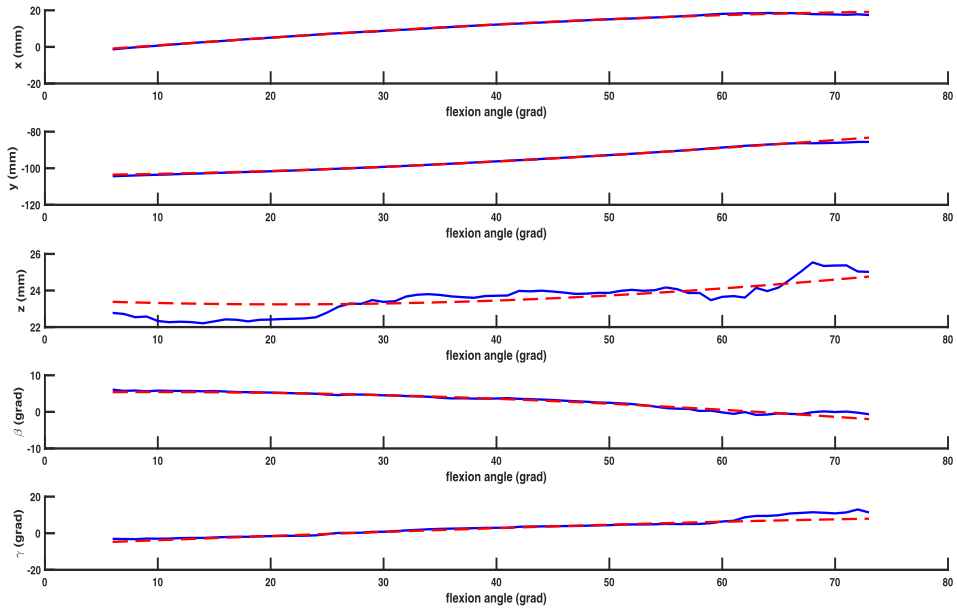

Figure 4.12 Pose parameters of the wrist and first phalange motion. Solid = experimental data; Dot = model. The model is identified by the B1 technique.

both the HA and B1 techniques, whereas for the B2 technique the values are slightly greater. Similar considerations can be given for the two rotational errors e_β and e_γ. In general, better results are mainly obtained for the relative motion between the bone 1 and 2, and for the relative motion between bone 2 and 3, whereas the results for the relative motion between bones 3 and 4 are in general the worst. However, except for some cases (e.g. for the relative motion between bones 3 and 4 of the ring finger), the results are very good.

It is worth noting that the results for both the HA and B1 techniques strongly depend on the choice of the pose to which the axis is associated. In particular, for the HA technique the choice to associate the axis to the pose at the 33% of the range of motion of the flexion angle, forces the error to be equal to zero in this particular pose, thus giving a great advantage (in terms of mean absolute error) to this technique with respect to the other two techniques base on the Burmester theory. Conversely, for the B2 technique the errors are greater but are pose-independent, thus are to be considered as the real-maximum errors committed by the revolute joint model.

Moreover, it is worth noting that, while the B1 technique compute the axis in-built to the fixed body by using all the BPs, the B2 technique splits the BPs

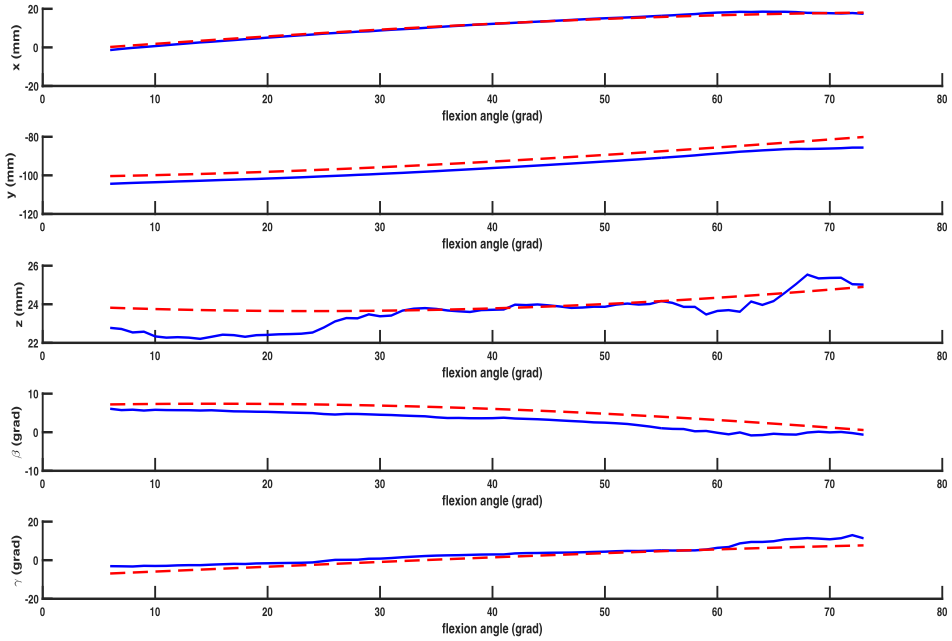

Figure 4.13 Pose parameters of the wrist and first phalange motion. Solid = experimental data; Dot = model. The model is identified by the B2 technique.

into two sub point cloud (one in-built to the fixed body and the other one in-built to the moving body), thus each one of the two resulting axes is computed with a fewer number of points. A deep analysis of the results obtained by the B2 technique reveals that the main source of errors is probably mainly due to a non-correct identification of the axis fixed to the moving body. However, to the best of the author's knowledge is not clear the origin of this problem.

Finally, as regards the relative motion between bones 3 and 4, the computed BPs are in general not well distributed along an axis of rotations (as they are for the relative motion between bones 1-2 and bones 2-3), but they are more thicken about a point than aligned about an axis, thus having a negative impact on the identification of a single axis of rotation.

Table 4.1 The computed errors for the HA, B1 and B2 techniques for the relative motion between all the adjacent bones of the three measured fingers. The labels *bone i-j* refers to the result obtained for the relative motion between the bone i and the bone j. Outside the brackets the absolute mean error is reported, whereas inside brackets the standard deviation of the mean absolute error is reported.

			e_x (mm)	e_y (mm)	e_z (mm)	e_β (grad)	e_γ (grad)
index finger	bones 1-2	HA	0.244 (0.329)	0.263 (0.484)	0.471 (0.308)	0.372 (0.508)	0.969 (1.460)
		B1	0.249 (0.341)	0.278 (0.467)	0.471 (0.310)	0.340 (0.494)	0.944 (1.376)
		B2	0.595 (0.436)	3.549 (0.439)	0.554 (0.507)	2.253 (0.576)	2.024 (1.201)
	bones 2-3	HA	0.259 (0.237)	0.504 (0.468)	1.250 (0.932)	1.009 (1.285)	3.034 (4.428)
		B1	0.136 (0.104)	0.146 (0.191)	2.180 (1.517)	1.722 (2.021)	3.866 (3.311)
		B2	0.393 (0.249)	2.282 (0.112)	1.652 (0.698)	1.574 (1.279)	3.947 (3.711)
	bones 3-4	HA	2.732 (1.864)	0.238 (0.190)	3.391 (2.059)	3.211 (4.494)	1.717 (2.152)
		B1	0.816 (0.732)	0.585 (0.503)	4.380 (3.065)	2.403 (3.722)	3.488 (3.348)
		B2	2.339 (0.975)	4.237 (0.453)	2.606 (1.336)	4.579 (5.000)	7.389 (2.345)
middle finger	bones 1-2	HA	0.268 (0.508)	0.507 (1.138)	0.691 (0.593)	1.592 (1.793)	0.435 (0.504)
		B1	0.705 (0.424)	0.649 (0.569)	0.462 (0.438)	1.922 (2.300)	0.778 (0.962)
		B2	0.896 (0.553)	1.503 (0.956)	0.291 (0.230)	11.835 (3.054)	8.571 (2.940)
	bones 2-3	HA	0.212 (0.162)	0.306 (0.282)	1.425 (1.066)	1.618 (2.561)	2.082 (2.586)
		B1	0.220 (0.210)	0.143 (0.159)	1.447 (0.928)	4.178 (4.382)	2.052 (1.924)
		B2	1.571 (0.730)	1.677 (0.242)	0.821 (0.569)	17.921 (1.835)	4.978 (5.370)
	bones 3-4	HA	0.226 (0.156)	0.547 (0.442)	1.663 (1.619)	5.356 (5.963)	2.341 (3.421)
		B1	0.471 (0.387)	0.393 (0.323)	1.692 (1.407)	5.447 (6.237)	2.426 (3.548)
		B2	0.931 (0.663)	0.260 (0.123)	1.494 (1.526)	17.739 (4.045)	18.813 (2.158)
ring finger	bones 1-2	HA	0.088 (0.083)	0.271 (0.295)	0.738 (0.448)	0.529 (0.670)	0.912 (1.237)
		B1	0.318 (0.239)	0.222 (0.290)	1.170 (0.736)	0.473 (0.608)	0.878 (0.980)
		B2	1.134 (0.545)	2.794 (0.282)	1.067 (0.702)	1.987 (0.609)	1.366 (0.996)
	bones 2-3	HA	0.232 (0.150)	0.863 (0.756)	1.364 (0.851)	1.375 (1.368)	1.480 (2.244)
		B1	0.165 (0.113)	0.214 (0.191)	1.459 (0.890)	1.178 (1.159)	1.045 (1.194)
		B2	2.305 (0.190)	0.566 (0.235)	1.504 (1.075)	7.031 (1.094)	2.482 (1.406)
	bones 3-4	HA	0.250 (0.199)	0.270 (0.208)	1.000 (0.686)	4.073 (4.023)	1.816 (2.195)
		B1	0.465 (0.359)	0.297 (0.274)	1.578 (1.123)	11.161 (13.231)	3.092 (1.815)
		B2	3.089 (0.675)	1.045 (0.671)	3.170 (1.071)	33.697 (9.784)	5.044 (4.802)

Conclusion

Recently, a prototype of a hand exoskeleton for post-stroke rehabilitation purpose, called Bologna Hand Orthoses (BHO), was proposed by the Group of Robotics, Automation and Articular Biomechanics (GRAB) at the Department of Industrial Engineering, University of Bologna. The BHO is mainly composed by two actuators, the first one simultaneously actuates the flexion/extension motion of the four fingers (the index, the middle, the ring and the little finger), whereas the second one actuates the flexion/extension motion of the thumb. Each finger is guided by a 1-DoF mechanism (a 12-link mechanism for the four fingers guidance, whereas an 8-link mechanism for the thumb guidance) directly coupled with the finger itself by Velcro® strips at the level of each human finger phalange. The moving link of the thumb mechanism is actuated by a RSSR mechanism whose frame link geometry changes according to the patient hand size.

With the future goal to build a new version of the BHO, in this dissertation three problems arising from this first prototype were tackled. In particular, the first problem regards the high number of human-machine connections needed to fasten the BHO to the patient hand, the second problem regards the synthesis of the RSSR mechanism in order to guarantee an optimal motion and force transmission to the thumb mechanism once the BHO is fitted to a new patient (i.e. for different frame link geometries of the RSSR mechanism), whereas the third problem regards the need to get a reliable model of the human hand.

The first problem has led to propose a new finger 1-DoF mechanism (in particular, a 6-link mechanism based on a Stephenson chain type) for the finger guidance that permits to lower the total number of human-machine connections from fifteen to only six. The new 6-link finger mechanism was here synthesized

for the index finger only, but the same synthesis procedure can be used for the synthesis of mechanisms useful for the guidance of all the five fingers. Moreover, several 6-link mechanisms ad hoc designed for the motion guidance of different finger sizes were found. Finally, several simulations with the aim to evaluate the behavior of the exoskeletons once fit on hands having a generic size are conducted. The simulations reveal encouraging results suggesting that the proposed finger exoskeleton can be successfully adopted for the motion guidance of the fingers for a hand exoskeleton.

As regards the second problem, a novel synthesis procedure for the optimal motion and force transmission of a RSSR mechanism was presented. The RSSR mechanism is characterized by having a fixed link length of the floating links and a variable frame link geometry. The proposed RSSR mechanism synthesis takes the optimization of the force transmission as an objective function. In addition, prescribed constraints on given extreme angular positions for both the moving and the follower links, on the upper and lower bounds for the transmission ratio, and on the upper and lower bounds for the floating link lengths values have to be satisfied. The synthesis problem, set as a constrained minimization problem, was solved numerically in two steps by means of a Genetic algorithm followed by a quasi-Newton algorithm. The synthesis procedure is firstly presented in a general way, and then applied to the RSSR mechanism of the BHO. The results show that an optimal RSSR mechanism can be found for a small range of frame link geometries and thus several considerations for a compromise solution were discussed.

Regarding the third problem, as a first step toward the modelling of the human hand was to model each finger as a serial manipulator and to approximate the flexion/extension motion of two adjacent bones as a rotation about a revolute axis. In this perspective, novel joint axes identification techniques were presented. The novel techniques are based on the Burmester theory. The Burmester theory is generally used for the synthesis of mechanisms, but it is used here in an original way to identify an axis of rotation. From this study two different joint axes techniques were proposed and a comparison of this two techniques with a more standard technique based on the finite helical axis was presented. Experimental tests devoted to measure in vivo the spatial motion of the index, middle and ring finger of a healthy subject were conducted. From the experimental test the relative motion between

adjacent bones of the human finger were obtained and the three joint axes techniques were applied. The results were very good and show that the identified axes of rotation by means of the three techniques are in general a very good approximation of the experimentally measured motion.

As a final remark, it is noteworthy that this dissertation reports different solutions for the modelling and design of a new version of the hand exoskeleton proposed by the GRAB, but it is worth noting that the problems here tackled and the solutions found are of general interest, thus going beyond the scope of this thesis.

Bibliography

Albrecht, I., Haber, J., and Seidel, H. P., (2003, July). Construction and animation of anatomically based human hand models. In *Proceedings of the 2003 ACM SIGGRAPH/Eurographics symposium on Computer animation*. Eurographics Association, 2003. p. 98-109.

Alizade, R. A., Freudenstein, F. and Pamidi, P. R., (1976). Optimum path generation by means of the skew four-bar linkage. *Mechanism and Machine Theory* 11(4): 295-302.

Alizade, R. I., and Sandor, G. N., (1985). Determination of the condition of existence of complete crank rotation and of the instantaneous efficiency of spatial four-bar mechanisms. *Mechanism and Machine Theory* 20(3): 155-163.

Bae, S., and Armstrong, T. J., (2011). A finger motion model for reach and grasp. *International journal of industrial ergonomics*, *41*(1), 79-89.

Balaji Rao, L. V., and Lakshminarayana, K., (1984). Optimal designs of the RSSR crank-rocker mechanism -I. General time ratio. *Mechanism and Machine Theory* 19(4-5): 431-441.

Balli, S. S. and Chand, S., (2002). Transmission angle in mechanisms (Triangle in mech). *Mechanism and Machine Theory* 37(2): 175-195.

Buchholz, B., Armstrong, T. J., and Goldstein, S. A., (1992). Anthropometric data for describing the kinematics of the human hand. *Ergonomics* 35(3): 261-273.

Buchholz, B., and Armstrong, T. J., (1992). A kinematic model of the human hand to evaluate its prehensile capabilities. *Journal of biomechanics* 25(2), 149-162.

Bullock, I. M., Borràs, J., and Dollar, A. M., (2012). Assessing assumptions in kinematic hand models: a review. In *Proceedings of the International Conference on Biomedical Robotics and Biomechatronics (BioRob)*, Rome, Italy, June 24-27, 2012: 139-146.

Burmester, L., (1877). Geradfuhrung durch das Kurbelgetriebe. *Civilngenieur* 23: 227-550.

Burton, T. M. W., and Vaidyanathan, R., (2010). A parameterized kinematic model of the human hand. *Towards Autonomous Robotic Systems (TAROS), Plymouth*: 34-40.

Burton, T. M. W., Vaidyanathan, R, Burgess, S. C., Turton A. J., Melhuish C., (2011). Development of a parametric kinematic model of the human hand and a novel robotic exoskeleton. *IEEE International Conference on Rehabilitation Robotics (ICORR).*

Cerveri, P., De Momi, E., Lopomo, N., Baud-Bovy, G., Barros, R. M. L., and Ferrigno, G., (2007). Finger kinematic modeling and real-time hand motion estimation. *Annals of biomedical engineering*, *35*(11): 1989-2002.

Chang, W. H., and Kim, Y.-H., (2013). Robot-assisted therapy in stroke rehabilitation. *Journal of stroke* 15(3): 174-181.

Chen, C., and Angeles, J., (2007). Generalized transmission index and transmission quality for spatial linkages. *Mechanism and Machine Theory* 42(9): 1225-1237.

Cobos, S., Ortego, J., Sanchez-Uran, M. A., Ferre, M., and Aracil, R., (2010). *Simplified human hand models for manipulation tasks*. INTECH Open Access Publisher.

Consoli, D., de Falco, F. A., Lenzi, G. L., Micieli, G., Palumbo, F., Rosati, G., Simonetti, G., Stanzione, P., Ugenti, R., and Zangrillo, A., (2010). Organizzazione dell'assistenza all'ictus: le Stroke Unit. *Italian Ministry of Health*.

Davidoff, N. A., and Freivalds, A., (1993). A graphic model of the human hand using CATIA. *International Journal of Industrial Ergonomics* 12(4), 255-264.

Grood, E. S., and Suntay, W. J., (1983). A joint coordinate system for the clinical description of three-dimensional motions: application to the knee. *Journal of biomechanical engineering* 105(2), 136-144.

Gupta, K. C., and Kazerounian, M. K., (1983). Synthesis of fully rotatable RSSR linkages. *Mechanism and Machine Theory* 18(3): 199-205.

Gustus, A., Stillfried, G., Visser, J., Jörntell, H., and van der Smagt, P., (2012). Human hand modelling: kinematics, dynamics, applications. *Biological cybernetics*, *106*(11-12), 741-755.

Heo, P., Min Gu, G., Lee, S.-J., Rhee, K., and Kim, J., (2012). Current hand exoskeleton technologies for rehabilitation and assistive engineering. *International Journal of Precision Engineering and Manufacturing* 13(5): 807-824.

Kapandji, I. A., (1983). *The Physiology of the Joints - Vol 1 - upper limb*. Elsevier Health Sciences.

Kazerounian, K. and Solecki, R., (1993). Mobility analysis of general bi-modal four bar linkages based on their transmission angle. *Mechanism and Machine Theory* 28(3): 437-445.

Innocenti, C., (1995). Polynomial solution of the spatial Burmester problem. *Journal of Mechanical Design* 117: 64-68.

Lee, S. W., and Zhang, X., (2005). Development and evaluation of an optimization-based model for power-grip posture prediction. *Journal of biomechanics*, *38*(8), 1591-1597.

Lenarcic, J., Bajd, T., and Stanišić, M. M., (2012). *Robot mechanisms* (Vol. 60). Springer Science & Business Media.

León, B., Morales, A., and Sancho-Bru, J., (2014). *From Robot to Human Grasping Simulation*. Springer, 2014.

Leonardis, D., Barsotti, M., Loconsole, C., Solazzi, M., Troncossi, M., Mazzotti, C., Parenti-Castelli, V., Procopio, C., Lamola, G., Chisari, C., Bergamasco, M., and Frisoli, A., (2015). An EMG-controlled robotic hand exoskeleton for bilateral rehabilitation. *IEEE Tranactions on Haptics* 8(2):140–151.

Liao, Q. and McCarthy, J. M., (2001). On the seven position synthesis of a 5-SS platform linkage. *Journal of Mechanical Design* 123(3): 74-79.

Loconsole, C., Leonardis, D., Barsotti, M., Frisoli, A., Solazzi, M., Bergamasco, M., Troncossi, M., Mozaffari Foumashi, M., Mazzotti, C., Parenti Castelli, V., (2013). An EMG-based robotic hand exoskeleton for bilateral training of grasp. In *Proceedings of IEEE World Haptics Conference (WHC)*, Daejeon (Korea), April 14-17, 2013, pp. 537-542.

Loureiro, R. C. V., and Harwin, W. S., (2007). Reach & grasp therapy: design and control of a 9-DOF robotic neuro-rehabilitation system. *IEEE International Conference on Rehabilitation Robotics (ICORR 2007)*, Twente, The Netherlands, June 13-15, 2007.

Malvezzi, M., Gioioso, G., Salvietti, G., and Prattichizzo, D., (2015). Syngrasp: A matlab toolbox for underactuated and compliant hands. IEEE *Robotics & Automation Magazine*, *22*(4): 52-68.

Marchal-Crespo, L. and Reinkensmeyer, D. J., (2009). Review of control strategies for robotic movement training after neurologic injury. *Journal of neuroengineering and rehabilitation* 6(1): 20.

Masia, L., Krebs, H. I., Cappa, P., and Hogan, N., (2007). Design and characterization of hand module for whole-arm rehabilitation following stroke. *IEEE/ASME Transactions on Mechatronics* 12(4): 399-407.

Mozaffari Foumashi, M., (2013). *Synthesis of Hand Exoskeletons for the Rehabilitation of Post-Stroke Patients*. PhD Dissertation, University of Bologna. web: http://amsdottorato.unibo.it/5906/.

Mozaffari Foumashi, M., Troncossi, M. and Parenti-Castelli, V., (2013). Design of a new hand exoskeleton for rehabilitation of post-stroke patients. Vienna. Springer: *Romansy 19–Robot Design, Dynamics and Control:* 159-166.

Mozaffari Foumashi, M., Troncossi, M., and Parenti-Castelli, V., (2011). State-of-the-art of hand exoskeleton systems. *Internal Report*, DIEM, University of Bologna.

Nolle, H., (1969). Ranges of motion transfer by the RGGR linkage. *Journal of Mechanisms* 4(2): 145-157.

Pheasant S., and Haslegrave C. M., (2003). *Bodyspace: Anthropometry, Ergonomics And The Design Of Work. Second Edition*. Taylor & Francis e-Library.

Sancisi, N., Parenti-Castelli, V., Corazza, F. and Leardini, A., (2009). Helical axis calculation based on Burmester theory: experimental comparison with traditional techniques for human tibiotalar joint motion. *Medical and Biological Engineering and Computing* 47(11): 1207-1217.

Sancisi, N., and Parenti-Castelli, V., (2013). Simultaneous Identification of the Human Tibio-Talar and Talo-Calcaneal Joint Rotation Axes by the Burmester Theory. In *ASME 2013 International Design Engineering Technical Conferences and Computers and Information in Engineering Conference*. Portland, Oregon, USA, August 4-7, 2013.

Siegel, A.F., (1982). Robust regression using repeated medians. *Biometrika* 69(1): 242-244.

Sutherland, G. and Roth, B., (1973). A transmission Index for Spatial Mechanisms. *Journal of Engineering for Industry* 95(2): 589-597.

Sutherland, G., (1981). Quality of motion and force transmission. *Mechanism and Machine Theory* 16(3): 221-225.

Takahashi Craig, D., Der-Yeghiaian, L., Le, V., Motiwala, R. R., and Cramer, S. C., (2008). Robot-based hand motor therapy after stroke. *Brain* 131.2: 425-437.

Rosati, G., Cenci, S., Boschetti, G., Zanotto, D., and Masiero, S., (2009). Design of a single-dof active hand orthosis for neurorehabilitation. *IEEE International Conference on Rehabilitation Robotics (ICORR 2009)*, Kyoto, Japan, June 23-26, 2009.

Troncossi M., Mozaffari Foumashi M., Carricato M., and Parenti-Castelli, V., (2012a). Feasibility study of a hand exoskeleton for rehabilitation of post-stroke patients. *In Proceeding of the 11th Biennial Conference on Engineering Systems Design and Analysis (ESDA 2012)*, Nantes, France, July 2 - 4, 2012.

Troncossi, M., Mazzotti, C., Mozaffari Foumashi, M., Zannoli, D., and Parenti-Castelli, V., (2012b). Design and Manufacturing of a hand-and-wrist exoskeleton prototype for the rehabilitation of post-stroke patients. *In Quaderni del DIEM Sesta Giornata di Studio Ettore Funaioli*. web: http://amsacta.unibo.it/3715/.

Tsai, M. J., and Lee, H. W., (1994). The transmissivity and manipulability of spatial mechanisms. *Journal of Mechanical Design* 116(1): 137-143.

Tsai, M. J., Lee, H. W., and Chen, H. C., (2011). Construction of a Realistic Hand Model with 22 Joint Freedoms. In *13th World Congress in Mechanism and Machine Science*.

Kapandji, I. A., (1982). *Physiology of the Joints: Upper Limb - Volume 1*. Edinburgh: Churchill Livingstone, 5-th edition.

Parasuraman, S., and Yee, K. C., (2009, March). Bio-mechanical analysis of human hand. In *Computer and Automation Engineering, 2009. ICCAE'09. International Conference on* (pp. 93-97).Bangkok, Thailand, March 8-10, 2009.

Pheasant, S., Haslegrave, C. M., (2003). *Bodyspace: Anthropometry, Ergonomics And The Design Of Work*. Taylor & Francis e-Library, 2-nd edition.

Rastegar, J., and Tu, Q., (1992). Approximated Grashof-type movability conditions for RSSR mechanisms with force transmission limitations. *Journal of Mechanical Design* 114(1): 74-81.

Rezzoug, N., and Gorce, P., (2008). Prediction of fingers posture using artificial neural networks. *Journal of biomechanics*, *41*(12), 2743-2749.

Şaka, Z., (1996). The RSSR mechanisms with partially constant transmission angle. *Mechanism and Machine Theory* 31(6): 763-769.

Sancibrian, R., De-Juan, A., Garcia, P., Fernandez, A., and Viadero, F., (2007). Optimal synthesis of function generating spherical and RSSR mechanisms. In *Proceedings of the 12th IFToMM World Congress*, Besançon, France, June 18-21, 2007.

Söylemez, E. and Freudenstein, F., (1982). Transmission optimization of spatial 4-link mechanisms. *Mechanism and Machine Theory* 17(4): 263-283.

Söylemez, E., (1993). Transmission optimization of right-angled four-bar mechanisms. *Mechanism and Machine Theory* 28(4): 539-552.

Soylu, R., (1993). Analytical Synthesis of mechanisms - part 1 transmission angle synthesis," *Mechanism and Machine Theory*, 28(6): 825-833.

Soylu, R., and Kanberoğlu, K. A., (1993). Analytical Synthesis of mechanisms - part 2. Crank-rotatability synthesis. *Mechanism and Machine Theory* 28(6): 835-844 .

Van Nierop, O.A., Van der Helm, A., Overbeeke, K. J. and Djajadiningrat, T. J. P., (2007). A natural human hand model. *Journal of the Visual Computer.*, 24(1): 31-44.

Veber, M., and Bajd, T., (2006, May). Assessment of human hand kinematics. In . *Proceedings of the IEEE International Conference on Robotics and Automation (ICRA 2006).* pp. 2966-2971. Orlando, Florida, USA, May 15-19, 2006.

Wolbrecht, E. T., Reinkensmeyer, D. J., and Perez-Gracia, A., (2011). Single degree-of-freedom exoskeleton mechanism design for finger rehabilitation. *IEEE International Conference on Rehabilitation Robotics (ICORR 2011)*, Zurich, Switzerland, June 29 - July 1, 2011.

Wu, G., Van der Helm, F. C. T., Veeger, H. E. J., Makhsous, M., Van Roy, P., Anglin, C., Nagels, J., Karduna, A. R., McQuade, K., Wang, X., Werner, F. W., and Buchholz, B., (2005). ISB recommendation on definitions of joint coordinate systems of various joints for the reporting of human joint motion-Part II: shoulder, elbow, wrist and hand. *Journal of biomechanics* 38(5): 981-992.

Yihun, Y., Miklos, R., Perez-Gracia, A., Reinkensmeyer, D. J., Denney, K., and Wolbrecht, E. T., (2012). Single Degree-of-Freedom Exoskeleton Mechanism Design for Thumb Rehabilitation. In *Proceedings of the Annual International Conference of the IEEE Engineering in Medicine and Biology Society (EMBC 2012)*. San Diego, USA, Aug 28 - Sep 1, 2012.

Appendix A

Human hand: anatomy and modelling

In this Appendix, a very short description of the human hand anatomy and of kinematic models of the human hand is given in order to lay down the basic terminology useful for a better comprehension of the Thesis.

Human hand anatomy

Starting from the shoulder, the upper limb is composed by the arm, the forearm and by the hand. The hand is composed by the wrist, that represents the continuity with the forearm, the metacarpus and the five fingers. The fingers are the thumb, the index, the middle, the ring and finally the little finger. The arm is composed by one bone, the humerus, whereas the forearm is composed by two bones, namely the radius and the ulna, finally the hand is composed by twenty seven bones subdivided in three mainly groups: the carpus, the metacarpus and the phalanges.

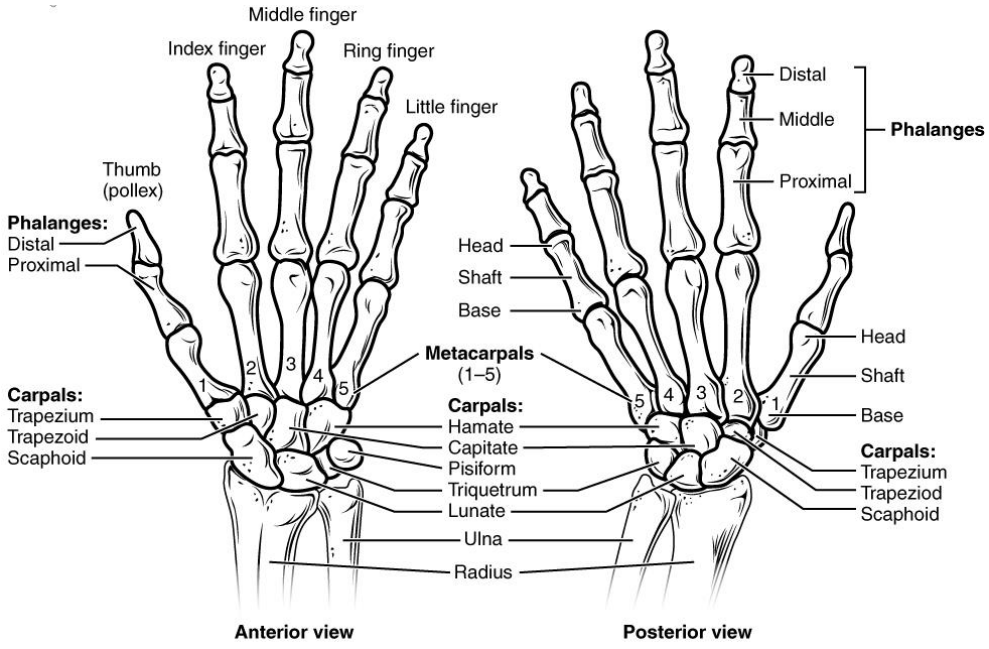

Figure A.1 The bones of the human hand.

Bones of the carpus

The carpus is composed by eight bones arranged in two rows, Figure A.1. The bones of the more proximal row, i.e. the bones closest to the forearm, proceeding in the radio-ulnar direction (i.e. the medial-lateral direction) are the scaphoid, the lunate, the triquetrum and the pisiform, whereas the bones of the second row are the trapezium, the trapezoid, the capitate and the hamate.

The scaphoid. It has three articular surfaces: one proximal for the contact with the radius, one distal for the contact with both the trapezium and the trapezoid and one medial for the upper contact with lunate and capitate.

The lunate. It has three articular surfaces: one proximal for the contact with the radius, one distal for the contact with both the hamate and the capitate and one lateral for the contact with the triquetrum.

The triquetrum. It has a proximal surface that is faced to the ulna and a distal surface for the contact with the hamate and the pisiform.

The pisiform. It has an articular surfaces faced to the hamate.

The trapezium. It has an articular surface for the contact with the capitate, a distal surface for the contact with the first metacarpal bone and finally a medial surface for the articulation with the second metacarpal bone.

The trapezoid. It has an articular surface for the contact with the scaphoid, a distal surface for the contact with the second metacarpal bone, a lateral surface for the contact with the trapezium and a medial surface for the contact with the capitate.

The capitate. It has a proximal surface for the contact with both the scaphoid and the lunate, a distal surface for the contact with the third metacarpal bone, a lateral surface for the contact with the trapezoid and a medial surface for the contact with the hamate.

The hamate. It has a proximal surface for the contact with the lunate, a distal surface for the contact with both the fourth and the fifth metacarpal bones, a lateral surface for the contact with the capitate and finally a medial surface for the contact with the triquetrum.

The radius-carpus joint (or wrist joint) is a condyloid joint. Its shape resembles an ellipse and thus permits movement in two planes, whereas the carpus-metacarpus joint is a synovial joint.

Bones of the hand: metacarpus and phalanges
The hand is composed by five metacarpal bones connected proximally with the carpus and distally with the phalanges of the fingers.
The metacarpus. These are five long bones whose proximally part is called the base, the middle part called the shaft (*diaphysis*) whereas the distal part is called the head (*epiphysis*). The first metacarpal bone, at the base is placed in contact with the trapezium, whereas distally is placed in contact with the thumb.
The base of the second metacarpal bone is in contact with both the trapezoid and the base of the third metacarpal bone.
The third metacarpal bone is in contact with the capitate bone and laterally and medially with the second and the fourth metacarpal bones respectively.
The fourth metacarpal bone is in contact with the hamate, the capitate and with both the third and the fifth metacarpal bones.
The fifth metacarpal bone is in contact with the fourth metacarpal bone and with the hamate.

The phalanges. These are three bones per finger, namely the proximal phalange, the medial phalange and the distal phalange, except for the thumb that had just two phalanges, i.e. the proximal and the distal one. As for the metacarpal bone, each phalange presents the base, the diaphysis and the distal epiphysis.
Each base of each proximal phalange is in contact with the corresponding epiphysis of each metacarpal bone, whereas the base of each medial phalange is in contact with the distal epiphysis of the corresponding proximal phalange, finally the base of each distal phalange is in contact with the corresponding medial phalange.

Each finger thus presents four bones connected through different joints, called from proximal to distal: *carpometacarpal* (CMC) joint, *metacarpophalangeal* (MCP) joint, *proximal interphalangeal* (PIP) joint and, *distal interphalangeal* (DIP) joint. The thumb, rather than the DIP and PIP joints only presents the *interphalangeal* (IP) joint, moreover, since the metacarpal bone of the thumb articulates with the *trapezium*, it is often equivalently referred to as the *trapeziometacarpal* (TM) joint instead of CMC joint.

The muscles producing movement of the fingers are divided into *extrinsic* and

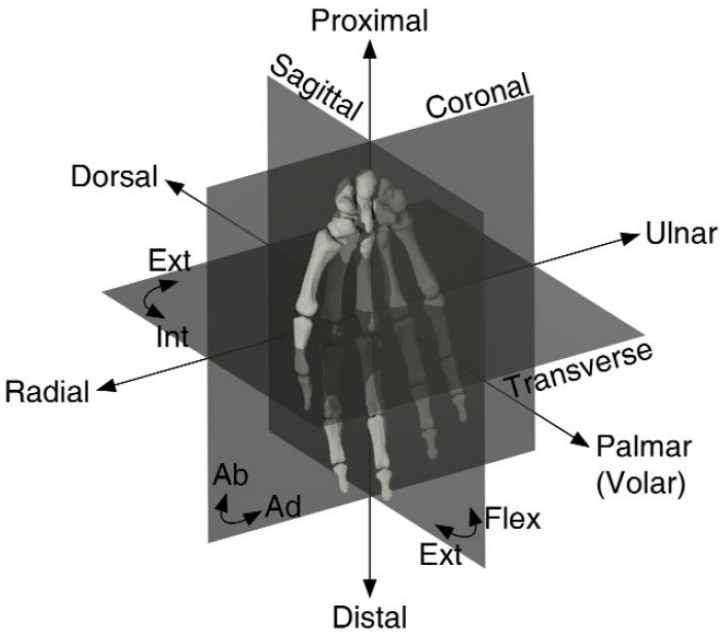

Figure A.2 Standard convention to describe the motion of the parts of the hand, taken from Bullock et al (2012).

intrinsic based on the origin of the muscles. The *extrinsic* muscles originate primarily in the forearm, while the *intrinsic* muscles originate primarily in the hand. The *extrinsic* muscles are divided into *flexors* found primarily on the anterior forearm and *extensors* found primarily on the posterior forearm. Both set of muscles insert on carpal bones, metacarpal or phalanges. The intrinsic muscles are divided into three groups: the *thenar*, the *hypothenar* and the *midpalmar* muscle groups.

In Figure A.2, a standard convention to describe the motion of the parts of the hand is illustrated. The intersection of the hand with the transverse, sagittal and coronal anatomical planes is shown, as well as the axes and rotation motions (referred to the three anatomical planes) are reported. The three main types of rotations are defined in terms of each of the three anatomical planes.

Human hand modelling

In the last decades, the human hand was studied for different purposes by hundreds of researchers, indeed in the literature there is a multitude of papers and books related to the hand. Certainly, the aim of this Section cannot be to provide a comprehensive review of all the works related to the human hand

modelling (perhaps, this is impossible), but rather to give the very basic elements useful for the next Chapters.

The hand has been considered as five skeletal open chains of rigid bodies connected to the carpus through different joints which characterise the kinematic behaviour of the chains. The DIP, PIP and IP joints of the fingers are trochlear joints, capable only of flexion/extension movements (Kapandji, 1983; Bullock et al., 2012). These joints are usually modelled as one DoF joints, in particular are revolute joints connecting the adjacent bones. All the MCP joints are condylar joints, thus capable of flex/extension and ab/adduction movements. The thumb CMC joint is a saddle joint, thus capable of flex/extension and ab/adduction movements. Both the MCP and CMC joints are usually modelled as two DOF joints by defining two revolute axes connecting the adjacent bones. In Table A.1, the universally-accepted assumptions for the kinematic model of the human hand in addition to the range of motion (RoM) of each articular joint are summarized. For a review of the common assumptions on the kinematic model of the human hand, see Bullock et al. (2012). A key-paper for the hand modelling is the work presented in Buchholz et al. (1992), where the finger was modelled as a serial manipulator having four segments and three articular joints, namely the MCP, PIP and DIP joint for the four fingers and TM, MCP and IP joint for the thumb. The link lengths of the serial manipulator correspond to the distance between two adjacent joints and Buchholz gives the corresponding average values as function of two independent parameters, i.e. the length and width of the human hand. Buchholz thus introduced the concept of scalability of the hand, and consequently his results are extensively used in the literature to scale the proposed models to different hands sizes. In the last decades, several researchers proposed a variety of kinematic models, e.g. Buccholz and Armstrong (1992), Davidoff et al. (1993), Albrecht et al. (2003), Lee and Zhang (2005), Veber and Bajd (2006), Cerveri et al. (2007), Van Nierop et al. (2007), Rezzoug and Gorce (2008), Parasuraman and Yee (2009), Bae and Armstrong (2011), Cobos et al. (2010), Burton et al. (2010), Tsai et al. (2011), Gustus et al. (2012), Lenarcic et al. (2012), Malvezzi et al. (2015). For a comprehensive review of the state-of-the-art of the human hand kinematic and biomechanics models let refers to the brilliant book of Leon et al. (2014).

Table A.1 Common assumptions for the kinematic model of the human hand. *DoF* stand for degree-of-freedom, whereas *RoM* stand for range-of-motion.

	Joint	*Type of joint*	*Model*	*Range of motion (RoM)*
thumb	TM	Saddle joint	Two non-orthogonal and non-coincident axes (2 DoFs). Also accepted the universal joint model.	Flex/extension : $-12° \div 50°$ Ab/adduction : $-30° \div 60°$
	MCP	Condylar joint	Two non-orthogonal and non-coincident axes (2 DoFs). Also accepted the universal joint model.	Flex/extension : $-10° \div 80°$ Ab/adduction : $-30° \div 60°$
	IP	Trochlear joint	Revolute joint (1 DoF).	Flex/extension : $-15° \div 80°$
index finger	CMC	Saddle joint	Usually considered as fix.	Flex/extension : $0°$
	MCP	Condylar joint	Universal joint (2 DoFs).	Flex/extension : $0° \div 90°$ Ab/adduction : $-15° \div 42°$
	PIP	Trochlear joint	Revolute joint (1 DoF).	Flex/extension : $0° \div 100°$
	DIP	Trochlear joint	Revolute joint (1 DoF).	Flex/extension : $-10° \div 90°$
middle finger	CMC	Saddle joint	Usually considered as fix.	Flex/extension : $0°$
	MCP	Condylar joint	Universal joint (2 DoFs).	Flex/extension : $0° \div 90°$ Ab/adduction : $-8° \div 35°$
	PIP	Trochlear joint	Revolute joint (1 DoF).	Flex/extension : $0° \div 100°$
	DIP	Trochlear joint	Revolute joint (1 DoF).	Flex/extension : $-10° \div 90°$
ring finger	CMC	Saddle joint	Usually considered as a revolute joint (1 DoF). Sometimes is considered as fix.	Flex/extension : $0° \div 15°$
	MCP	Condylar joint	Universal joint (2 DoFs).	Flex/extension : $0° \div 90°$ Ab/adduction : $-20° \div 14°$
	PIP	Trochlear joint	Revolute joint (1 DoF).	Flex/extension : $0° \div 100°$
	DIP	Trochlear joint	Revolute joint (1 DoF).	Flex/extension : $-20° \div 90°$
little finger	CMC	Saddle joint	Usually considered as a revolute joint (1 DoF). Sometimes is considered as fix.	Flex/extension : $0° \div 30°$
	MCP	Condylar joint	Universal joint (2 DoFs).	Flex/extension : $0° \div 90°$ Ab/adduction : $-40° \div 19°$
	PIP	Trochlear joint	Revolute joint (1 DoF).	Flex/extension : $0° \div 100°$
	DIP	Trochlear joint	Revolute joint (1 DoF).	Flex/extension: $-30° \div 90°$